14

Ukar, Estibalitz, Ramiro G. López, Damian Hryb, Julia F. W. Gale, René Manceda, András Fall, Ignacio Brisson, Eider Hernandez-Bilbao, Ralf J. Weger, Denis A. Marchal, Alain Zanella, and Peter R. Cobbold, 2020, Natural fractures: From core and outcrop observations to subsurface models, *in* Daniel Minisini, Manuel Fantín, Iván Lanusse Noguera, and Héctor A. Leanza, eds., Integrated geology of unconventionals: The case of the Vaca Muerta play, Argentina: AAPG Memoir 121, p. XX–XX.

Natural Fractures: From Core and Outcrop Observations to Subsurface Models

Estibalitz Ukar, Julia F. W. Gale, and András Fall

Bureau of Economic Geology, Jackson School of Geosciences, The University of Texas at Austin, University Station Box X, Austin, TX 78713-8924, USA (e-mails: esti.ukar@beg.utexas.edu; julia.gale@beg.utexas.edu; andras.fall@beg.utexas.edu)

Ramiro G. López and Damian Hryb

YPF S.A., Macacha Güemes 515, C1106BKK Buenos Aires, Argentina (e-mails: ramiro.lopez@ypf.com; damian.hryb@ypf.com)

René Manceda

RM Geostructural Consulting, Alicia Moreau de Justo 846-4-14, Caba, 1107, Argentina (e-mail: rmanceda@outlook.com)

Ignacio Brisson

YPF S.A., Macacha Güemes 515, C1106BKK Buenos Aires, Argentina (e-mail: ignacio.brisson@ypf.com)

Eider Hernandez-Bilbao

Total CSTJF, Avenue Larribau, 64000 Pau, France (e-mail: eiderhdez@gmail.com)

Ralf J. Weger

CSL – Center for Carbonate Research, Rosenstiel School of Marine and Atmospheric Science, University of Miami, 4600 Rickenbacker Causeway, Miami, FL 33149, USA (e-mail: rweger@rsmas.miami.edu)

Denis A. Marchal

Pampa Energia S.A., Maipu 1, CP1084, Ciudad Autónoma de Buenos Aires, Argentina (e-mail: denis.marchal@pampaenergia.com)

Alain Zanella

Géosciences Le Mans, UMR 6112 CNRS, Le Mans Université, Avenue Olivier Messiaen, 72085 Le Mans Cedex 9, France (e-mail: alain.zanella@univ-lemans.fr)

Peter R. Cobbold

Géosciences Rennes UMR6118, CNRS and Université de Rennes 1, 35042 Rennes, France (e-mail: peter.cobbold@univ-rennes1.fr)

 DOI: 10.1306/13682234M1203837

ABSTRACT

Natural fractures are abundant in the Vaca Muerta Formation and are important because they may affect hydraulic-fracture growth during well stimulation. They contribute to anisotropic mechanical behavior of the reservoir rock and may cause hydraulic fractures to arrest or divert along them by opening or shear. In the subsurface, the Vaca Muerta Formation contains bed-parallel veins (BPV) of fibrous calcite (beef) and bed-perpendicular, completely or partly calcite-filled, opening-mode fractures in multiple orientations. In outcrops of the Vaca Muerta Formation in the Agrio fold-and-thrust belt, BPV and bed-perpendicular fractures are also common. Fracture cement geochemistry (including stable isotopes) and fluid inclusion and clumped isotopic thermometry indicate that the outcrops are similar to the most mature parts of the Vaca Muerta reservoir and can be used as guides for this part of the basin. In outcrops near the Cerro Mocho area, two main bed-perpendicular, opening-mode fracture sets are oriented east–west (oldest) and north–south (youngest), and two additional sets (northeast–southwest and northwest–southeast) are locally present. Fluid inclusion microthermometry, combined with burial-history curves, indicates that BPV in the area of Loncopué formed in the Late Cretaceous during bed-parallel contraction and in overpressure conditions, whereas bed-perpendicular sets formed in the Paleocene. Similar ages were obtained for Puerta Curaco outcrop on the basis of clumped isotope temperatures, although BPV opening may have lasted until the Miocene in this area. BPV are the most common and some of the oldest types of fracture sampled by vertical cores, and stable isotope analyses indicate that they formed deep in the subsurface, probably under conditions similar to those inferred for outcrops. In cores of the Loma Campana block, bed-perpendicular fractures show orientations similar to those in outcrops, although the youngest, north–south set is generally missing. Without appropriate fluid inclusions for microthermometry or oriented cross-cutting relationships in core, fracture timing was established on the basis of a tectonic model. Our model indicates that in the Loma Campana block, fractures preferentially formed in east–west and northeast–southwest orientations in the Early Cretaceous, northeast–southwest in the Late Cretaceous, northwest–southeast in the Cenozoic, and east–west and east-northeast–west-southwest at present. Fracture timing and orientations from this tectonic model, fracture aperture from core, fracture height and length measured in outcrop, and fracture intensity from a geomechanical model calibrated with core and image logs were used to construct discrete fracture network (DFN) models of the subsurface and build specific reservoir development plans.

INTRODUCTION

Natural fracture systems are present in most self-sourced unconventional reservoir rocks (Gale et al., 2014). Their influence on fluid flow in the subsurface, and on hydrocarbon production, is challenging to quantify because there are several variables to consider including size, extent of mineral cement fill, and orientation relative to the in situ stress field. Fractures with cement linings on their walls, but which are otherwise open, can enhance permeability. Because openness is size dependent (Laubach, 2003), and fractures commonly follow power-law aperture size distributions (Marrett et al., 1999), open fractures are much less common than their sealed counterparts. Sealed fractures, however, are not necessarily barriers to fluid flow. In a study of natural, calcite-filled fractures in the Eagle Ford Formation (South Texas, USA), Landry et al. (2016) found that permeability of cement fill is comparable to that of the host rock. Moreover, fracture cement modeling of quartz cement accumulation in opening fractures predicts barren fractures for mudrocks (at least with respect to quartz) if there is no substrate for quartz to nucleate on (Lander and Laubach, 2015). The majority of natural fractures in mudrocks, therefore, may present neither pathways nor barriers to fluid flow (in the other chapters of this Memoir "mudrock" may be substituted for "mudstone").

Natural fractures are potentially important partly because they may interact with hydraulic fracture stimulation treatments (Warpinski et al., 2005; Gale et al., 2007; Jeffrey et al., 2009). Preexisting discontinuities, including natural fractures, may have low strength relative to the host rock, possibly causing perturbations in the local stress field and contributing to anisotropic elastic behavior of the rock mass. These discontinuities can reactivate by opening or shear during hydraulic fracturing, or they may arrest hydraulic fracture growth (Zhang et al., 2009, 2017; Lee et al., 2015).

Structural diagenetic studies of fractures can help establish the characteristics, origin, and timing of formation of different fracture sets as well as the tectonic history of the reservoir, which is fundamental for understanding the generation of the petroleum system. Information derived from these studies can be used to iteratively calibrate discrete fracture network (DFN) models of the reservoir, which are essential to hydraulic fracture interaction prediction. Although challenging, incorporation of such fractures is critical, especially in low-permeability reservoirs such as the Vaca Muerta Formation (Du et al., 2011). Cores are three-dimensional (3-D) objects, but at the reservoir scale they are effectively one-dimensional (1-D) because the diameter is much smaller than the length. Fractures are mostly taller and longer than the core diameter so that their height and length are challenging to measure (e.g., Lerche and Narr, 1986).

A good approach to reservoir characterization is to combine outcrop and core information. With this approach, establishing at least some characteristics of the outcrops to reflect the fracture system in the subsurface becomes essential (Ukar et al., 2019). A key element is timing of fracture growth; fracture sets are first identified on the basis of orientation and cross-cutting relationships and then further constrained using fluid inclusions and burial-history models. The fracture sets so identified may be related to tectonic events and overpressuring during the basin's history. Establishing the timing of formation of different fracture sets can help decrease the degree of uncertainty of subsurface models, whereas establishing accurate temperatures for the formation of different fracture sets enhances our ability to understand their relationship to hydrocarbon maturation.

The Vaca Muerta Formation is known to host many natural fractures, which have been well documented in core (Hernandez-Bilbao, 2016; Marchal et al., 2016; de Barrio et al., 2018; Palacio et al., 2018), cuttings (Martinez et al., 2017), and outcrop (e.g., Rodrigues et al., 2009; Zanella et al., 2015; Ukar et al., 2017b, c; Weger et al., 2019). The interaction of hydraulic fractures with natural fractures, specifically in the Vaca Muerta Formation, has also been addressed (e.g., Monti et al., 2013; Haddad et al., 2017), although natural fractures are represented in these studies in a simplified manner.

In this chapter, we provide an overview of natural fracture types and their characteristics in the Vaca Muerta Formation. We compare fractures in core and in outcrop across the Neuquén Basin. Using fracture cements that preserve information on fluids in the basin at the time of cement precipitation, we infer conditions of fracture formation. We report fracture size (aperture, length, and height), spacing, fill, relationship to faults, and fluid inclusion temperatures and infer relative and absolute fracture timing. We define macrofractures as those fractures that can be observed without a visual aid (typically >0.1 mm in aperture) and microfractures as those that require microscopy. In field data sets we measured all sealed fractures but also included apparently barren fractures having the same orientation as adjacent sealed fractures. Image log data sets include nonconductive (sealed) and conductive (open) fractures, and these were counted as natural fractures except for those conductive fractures with orientations and morphologies consistent with a drilling-induced origin, which were separated out. We discuss an example of subsurface characterization that is based on 3-D seismic structural interpretation, cores, image logs, and outcrop observations subsequently coupled with geomechanical models, resulting in representative and realistic DFN models. Such models are powerful tools that can aid in the accurate prediction of key natural fracture attributes, such as fracture abundance and orientation, both of which may have a strong impact on hydrocarbon production, thus helping to improve well completion design, well stimulation, and reservoir development.

GEOLOGIC SETTING

Mesozoic strata of the Neuquén Basin accumulated during a complex tectonic history related to evolution of the western margin of Gondwana (Ramos et al., 2020, this Memoir). Late Triassic to Early Jurassic rifting controlled the evolution of the basin allowing development of large half-grabens. The postrift stage consisted of several contractional and minor Pliocene extensional events (Pardo-Casas and Molnar, 1987; Vergani et al., 1995; Mosquera and Ramos, 2005). Several factors resulted in a complex tectonic history, including tectonic inversion in most of the fold-and-thrust belt and reactivation of basement faults in the foreland area and rotation of the maximum compressive horizontal stress from the Jurassic, when the subduction system was initiated, with a stress vector of about N160° (Mosquera and Ramos, 2005) to the current stress vector of N075° (Pardo-Casas and Molnar, 1987; Brooks et al., 2003; Guzmán, 2007).

The postrift stage was characterized by deposition of the Cuyo and Lotena Groups, which were exposed as a result of Late Jurassic inversion related to the Araucanian event (Leanza, 2009). In the Kimmeridgian, the Tordillo Formation was deposited unconformably. Following a sea-level drop, the Tordillo Formation was reworked in fluvial systems along the basin margins forming eolian and lacustrine deposits in the basin center (Marchese, 1971; Arregui, 1993). At the beginning of the Tithonian, most of the continental margin was flooded from the Panthalassa Ocean triggering deposition of a basin-wide, extremely organic-rich unit at the base of the Vaca Muerta Formation. Marine transgression was followed by a regression giving place to a prograding clinoform up to 1700 m (5577 ft) thick—the Vaca Muerta–Quintuco System (Mitchum and Uliana, 1985; Kietzmann et al., 2020, this Memoir). The Quintuco Formation represents the topset of the clinoform, whereas the Vaca Muerta Formation represents the foreset and bottomset.

The Vaca Muerta Formation comprises marine mudrocks (sedimentary rocks having a dominant grain size of <65 µm; Loucks et al., 2009) and marlstones deposited under anoxic conditions interbedded with thinner limestones and volcaniclastic layers (i.e., tuffs or bentonites). This formation underlies most of the foreland basin and is the main source rock for oil and gas in the Neuquén Basin because of its high organic content (as much as 10%–12% total organic carbon [TOC] at the base) (Urien and Zambrano, 1994; Cruz et al., 1996). The organic-rich layer at the base constitutes one of the main landing zones of the unconventional play. Today the Vaca Muerta Formation is exposed in the foothills of the Andes, mainly in cores of anticlines and hanging walls of thrust faults. This thin-skinned deformation is overprinted on thick-skinned structures of reactivated basement faults that were transported eastward and inserted beneath an Upper Jurassic décollement (Zapata et al., 1999; Zamora Valcarce et al., 2006). Strata are inferred to have been exhumed from about 4 km (2.5 mi) depth in two episodes: an older event between 90 and 50 Ma and another between 11 and 6 Ma (Zamora Valcarce et al., 2009).

Outcrop findings documented in this chapter are from (1) the western Agrio fold-and-thrust belt in the Cerro Mocho area, about 10 km (6 mi) east of the Loncopué Trough, (2) the east part of the Malargüe fold-and-thrust belt in the Puerta Curaco (PC) and nearby Yesera del Tromen (YdT) areas 30 km (19 mi) east of Chos Malal, (3) the area of Mallin Quemado in the northernmost part of the Sierra de la Vaca Muerta (SdlVM), and (4) the approximately east–west asymmetric Picún Leufú anticline located about 30 km (19 mi) south of Zapala (Figure 1).

The Loncopué area has a complex tectonic history involving several contractional phases from Early Cretaceous to Neogene and one important extensional phase in the Oligocene. The Arroyo Mulichinco, Puesto, and Arroyo Huncal outcrops are part of an area characterized by a series of north–south-trending anticlines (Figure 2). At Arroyo Mulichinco, studied exposures are near a bridge, along the bottom of a creek, where strata dip gently to the southeast. At Puesto, fractures were analyzed along the bottom of a dry creek and in cliffs 10 to 20 m (33–66 ft) tall. Here, strata generally dip from 10° to 25° to the west-northwest–northwest, and mesofaults are common (Ukar et al., 2017a, b). About 150 m (492 ft) of the basal Vaca Muerta Formation are exposed at Arroyo Huncal, where strata dip about 25° to the east (Spalletti et al., 1999; Leanza, 2003).

Near PC, the exposed Vaca Muerta Formation represents the basinal part of the Late Jurassic–Early Cretaceous transgression, and it is composed mainly of mixed carbonate siliciclastic mudstones and limestones (Legarreta and Gulisano, 1989). These outcrops are on the western side of the La Yesera anticline. In the SdlVM, Tordillo and Vaca Muerta formations are exposed on an approximately 35-km (22-mi)-long, north–south-trending, partly eroded anticline that allows exceptional insights into the stratal architecture of the middle Tithonian to Berriasian deposits (Zeller et al., 2015). The Picún Leufú anticline provides excellent exposure of the Tithonian to Berriasian mixed successions of the Vaca Muerta–Quintuco System (Leanza, 1973; Spalletti et al., 2000; Armella et al., 2007; Leanza et al., 2011; Zeller et al., 2015), but in this area, fractures and faults are rare.

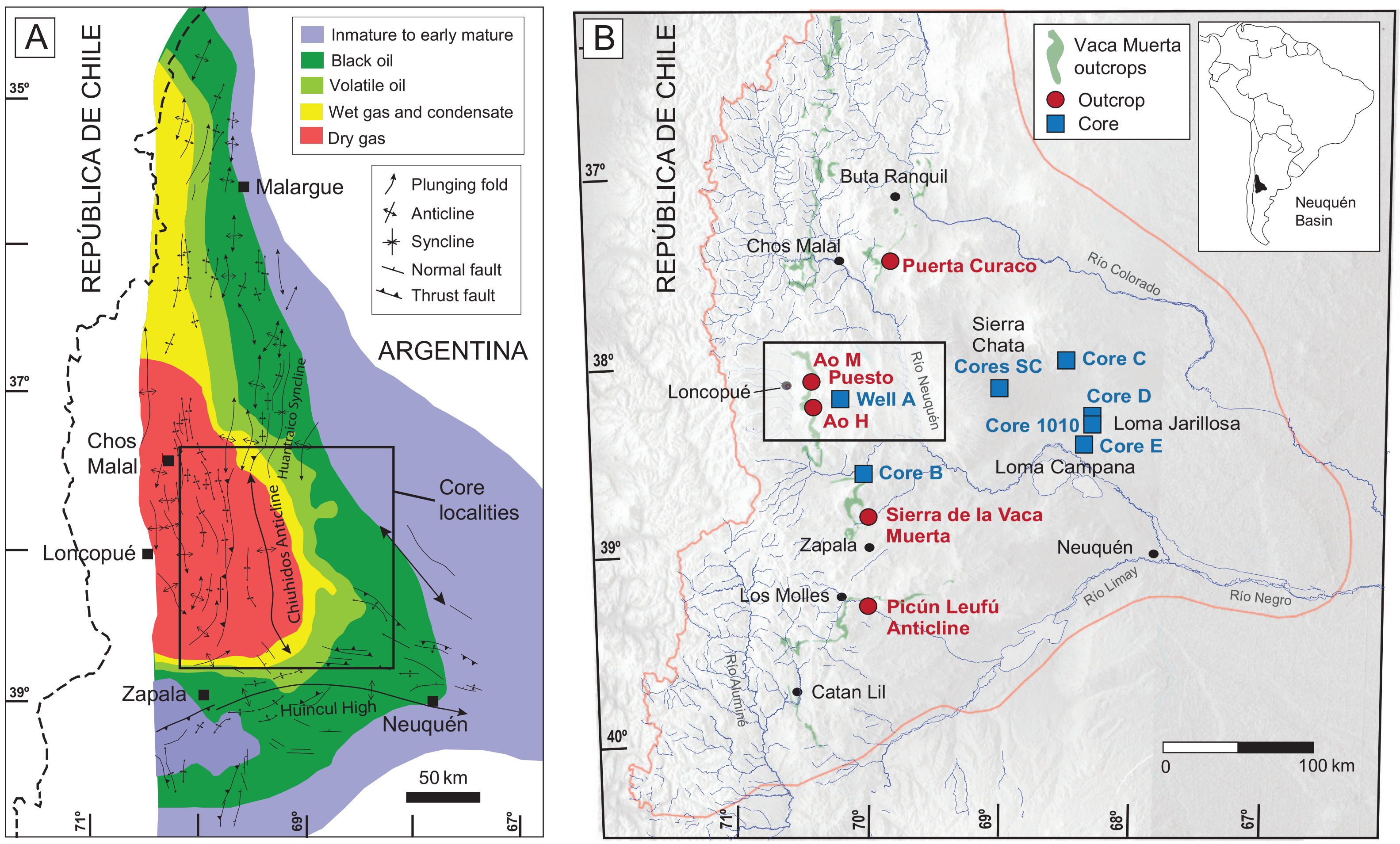

Figure 1. Tectonic setting of Neuquén Basin showing outcrop and core locations. (A) Map showing orientation of main structures and distribution of fluid segments within the Vaca Muerta play. After Legarreta and Villar (2011) and Gutiérrez-Schmidt et al. (2014). (B) Location of Vaca Muerta Formation outcrops and cores mentioned in this study. Rectangle shows the location of Figure 2. Ao M = Arroyo Mulichinco; Ao H = Arroyo Huncal.

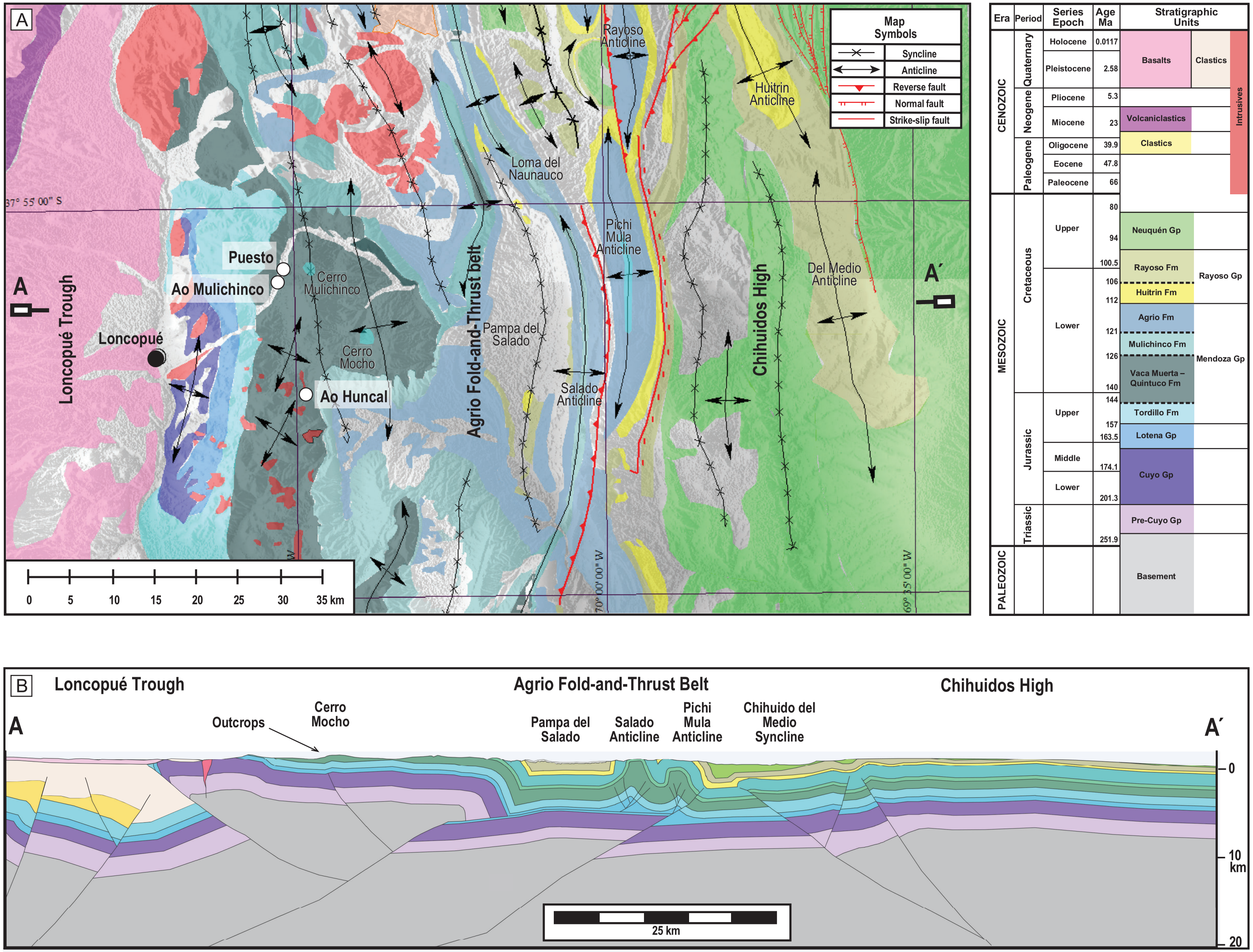

Figure 2. (A) Geologic map showing location of Arroyo Mulichinco, Puesto, and Arroyo Huncal outcrops (after Rojas Vera et al., 2014). (B) Cross section of Loncopué area.

This chapter also discusses data from 18 wells from an area approximately 200 km (124 mi) east of the Loncopué outcrops (Figure 1). Cores from six of these wells (B, C, D, E, 1010, and SC) were studied in more detail, especially those in the Loma Jarillosa, Sierra Chata, and Loma Campana areas, the latter of which being used in the construction of tectonic and DFN models described in this chapter. Core 1010 is from the east-central part of the Neuquén Basin in the area of the Loma Jarillosa Este block, northeast of the Loma La Lata block (Figure 1B). This area is located in the foreland, within the Añelo depocenter just south of the Eastern Platform and Catriel Shelf and north of the Añelo Trough and Huincul High. The nearby Core E is from the 10-by-10 km (6-by-6 mi) Loma Campana block. Several reactivated basement faults controlled and subsequently folded syn-rift growth strata during the Mesozoic, and a series of gentle anticlines are observed in the subsurface (Figure 3). The Sierra Chata area is located to the west, on the east side of the Chihuidos High (Figures 1, 2). Data from this area are from two cores, as described by Marchal et al. (2016) and de Barrio et al. (2018). In the Sierra Chata block, the Vaca Muerta–Quintuco System is slightly deformed, and strata dip approximately 3° to the north-northwest, increasing to an average of 6° in the foreset part of the clinoforms, except for a kilometer-scale slump feature in the southeastern sector of the block (Marchal et al., 2016).

Across most of the Neuquén Basin, the Vaca Muerta Formation is in the oil-to-gas window and has reached the gas window in the foothills (Kozlowski et al., 1998; Gutiérrez-Schmidt et al., 2014) (Figure 1A). Outcrops near the Loncopué Trough were affected by high heat flow in the Oligocene that was caused by asthenospheric upwelling into this tectonic window (Pesicek et al., 2012; Rojas Vera et al., 2014, 2015). Thermal maturity of the Vaca Muerta Formation in this area is therefore higher than from burial alone. Out of the 18 cores studied, 14 are farthest away from outcrops and are in the oil window, whereas 4 are only a few tens of kilometers away from outcrops and have reached similar temperature and pressure conditions in the gas window, including the two Sierra Chata (SC) cores (Figure 1).

TECTONIC SETTING

The western margin of South America comprises a multiphase deformation system that includes stages of rifting, postrift, several phases of inversion, postinversion, foreland formation, and Andean tectonics (Zonenshayn et al., 1984; Jaillard et al., 1990; Scheuber et al., 1994; Mosquera and Ramos, 2005) caused by changes in relative plate motion (see also Marchal et al., 2020, this Memoir). At about 160 Ma, convergence between the South American and Aluk plates was north-northwest (Mosquera and Ramos, 2005). In the Cretaceous, emplacement of the Farallon plate against the South American margin caused compression to change to east–west and then northeast–southwest (Mosquera and Ramos, 2005), although this shift is not well constrained owing to the absence of oceanic crust of this age on the Nazca plate. At the beginning of the Tertiary, oblique convergence became progressively more orthogonal during the Neogene (Pardo-Casas and Molnar, 1987; Somoza, 1998). Fastest convergence occurred in the Aptian–Albian (Peruvian phase), Eocene (Incaica phase), and Late Oligocene–Early Miocene (Quechua phase) (Cobbold and Rossello, 2003).

FRACTURES IN OUTCROP

Opening-mode fractures are traditionally referred to as veins or joints based on the presence or absence of mineral deposits, respectively. However, the degree of cement fill is in many cases dependent on size (e.g., Lander and Laubach, 2015), where small fractures (microfractures <0.1 mm in aperture) of a given set are usually completely infilled with cement (veins), whereas their larger counterparts may be completely barren (joints). We use the unambiguous descriptive term "fracture" to refer to opening-mode fractures with varying amount of cement fill and "faults" for those fractures that show shear displacement.

Bed-Parallel Fractures in Outcrop

In Early Tithonian–Early Valanginian Vaca Muerta Formation outcrop exposures, bed-parallel veins (BPV) of fibrous calcite (beef) are common (Rodrigues et al., 2009; Cobbold et al., 2013; Zanella et al., 2015; Ukar et al., 2017b) (Figure 4). The term "beef" was first coined by Buckland and De La Bèche (1835) in the Wessex Basin of Southern England where they described "Shales-with-Beef". However, not all BPV are filled with fibrous calcite, so we use the more general term "BPV." Similar BPV have been reported in sedimentary basins around the world, especially in organic-rich mudrocks, the so-called "black shales" (Tobin et al., 1996; Cobbold et al., 2013; Gale et al., 2014; Zanella et al., 2020). In our study areas, BPV vary from a few millimeters to about 10 cm (4 in.) in thickness and may extend laterally for several centimeters to decimeters or for several hundreds of meters. Weger et al. (2017) reported an approximately 10-cm

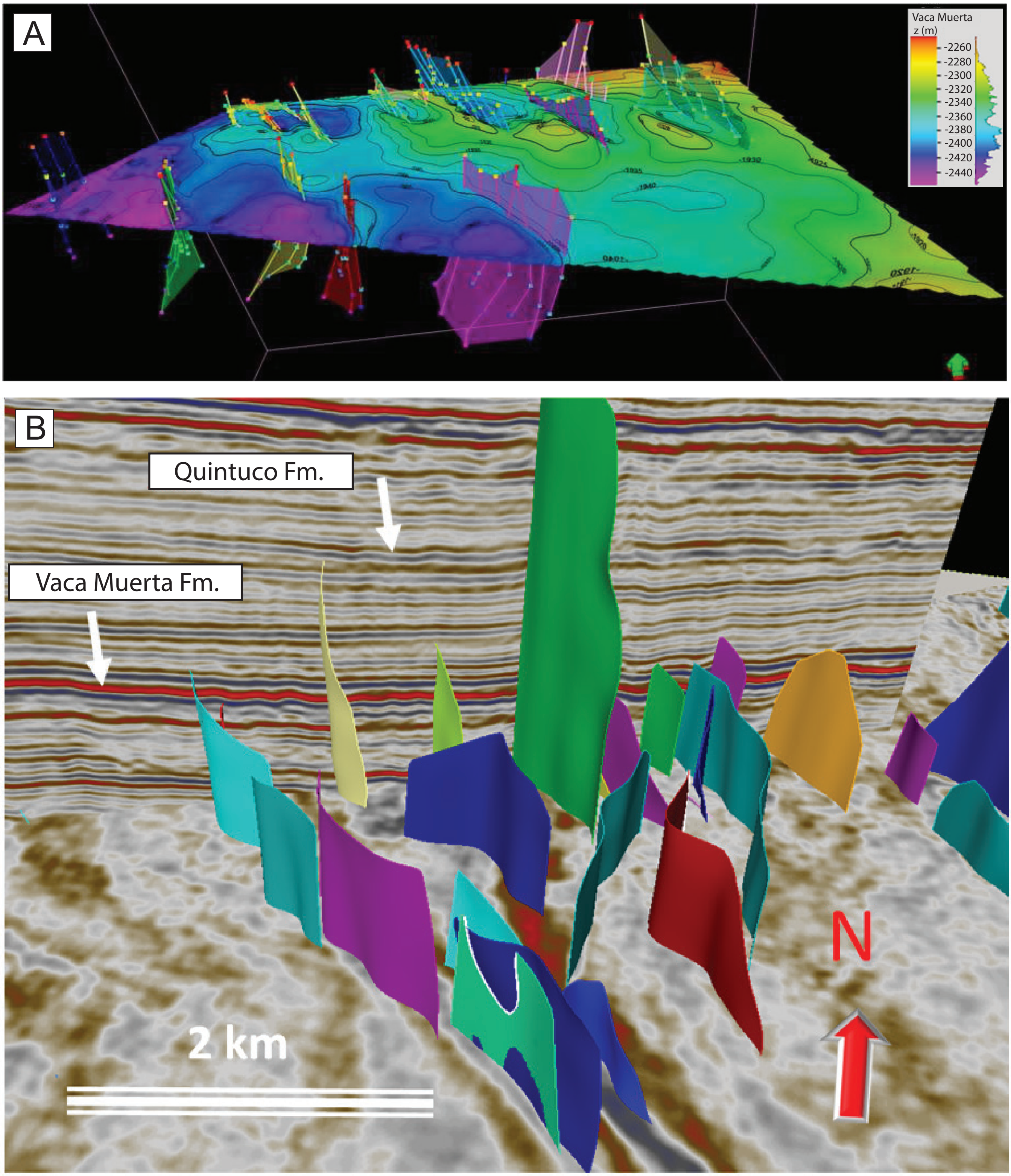

Figure 3. Seismic images with orientation of main fault planes in subsurface. (A) Structural map of top of Vaca Muerta Formation showing north-northwest–south-southeast normal faults and grabens in the Loma Jarillosa block (Franklin, 2016), 5 m (16 ft) contour intervals. Area shown is approximately 10 km (6 mi) wide. (B) Faults in Loma Campana block with orientations similar to those in Loma Jarillosa. Arrows indicate Vaca Muerta and Quintuco Formation reflectors.

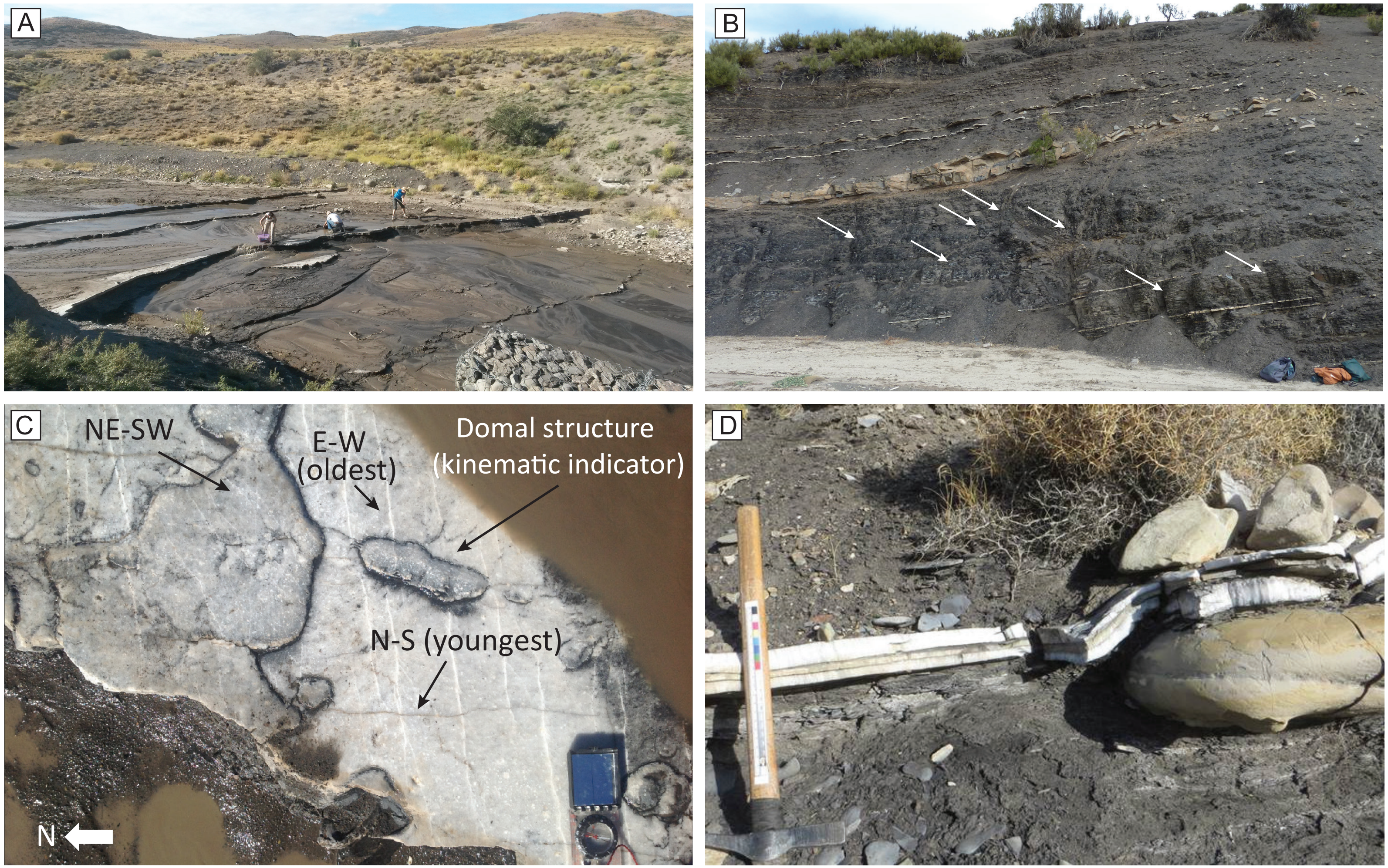

Figure 4. Photographs of Vaca Muerta Formation outcrops. (A) Arroyo Mulichinco with prominent BPV. (B) Puesto with BPV and calcite-filled, bed-perpendicular fractures in mudrock (arrows). Bed-perpendicular fractures in some cases cut and in others abut against BPV. (C) Calcite-filled, bed-perpendicular fractures cutting BPV and domal structures (kinematic indicators) within BPV at Arroyo Mulichinco. Three of the four main fracture orientations (east–west, northeast–southwest, northwest–southwest, north–south) are shown. After Ukar et al. (2017b). Fracture orientations similar at Puesto. (D) BPV associated with concretion at Puerta Curaco. Many BPV are associated with concretions because they constitute mechanical interfaces where BPV nucleate. BPV = bed-parallel veins.

(4-in.)-thick BPV with lateral continuity exceeding 1 km (0.6 mi) at PC.

Loncopué outcrops contain some of the most abundant (~10% of the volume of the formation; Rodrigues et al., 2009), thickest, and most laterally continuous BPV in the world. In PC, BPV are concentrated mostly in two intervals: the upper Tithonian to middle Berriasian interval and the lower Valanginian (constituting ~4% of the volume of the formation; Weger et al., 2019), whereas at SdlVM and Picún Leufú, BPV are scarce or very thin, with the exception of the area of Mallin Quemado, where they abound.

Most BPV contain inclusions of host rock, bitumen, and pyrite (Rodrigues et al., 2009) and a thin layer of host rock fragments along the center, termed the "median line" in 2-D sections (Passchier and Trouw, 1996) (Figure 5A–C). Growth of calcite is generally antitaxial from the median line, and in most cases, there are two or more generations of fibers (Figure 5A–C). Thickness of the BPV on opposite sides of the median line may differ, resulting in off-centered lines in some cases (Figure 5A). In many BPV, calcite fibers adjacent to the median line are mainly orthogonal to the layer and symmetrical (Figure 5B). In this inner zone (zone 1), calcite fibers are nearly vertical after bedding is restored to horizontal. Away from the center, BPV contain inclined calcite fibers, oblique to bedding, indicating shear during BPV opening. In some BPV, the direction of inclination of these outer fibers is the same at the top and bottom of the BPV, plunging toward the west–west-northwest at Arroyo Mulichinco (Ukar et al., 2017b). In other examples, fibers in the outermost part of the BPV dip in opposite directions (Rodrigues et al., 2009). We also found many examples that differ from the orthogonal inner- and inclined outer-zone geometry mentioned earlier, and BPV completely lacking a median line.

Most BPV contain U- or V-shaped host rock fragment arrays intercalated within calcite fibers termed "cone-in-cone" structures (Figure 5C). Such structures were first described by Buckland and De La Bèche in 1835 in the Shales-with-Beef Formation, and they are common in BPV around the world (e.g., Cole, 1893; Franks, 1969; Cobbold et al., 2013; Hooker and Cartwright, 2016; Maher et al., 2016). The mechanisms of formation of such internal structures are not yet well understood although they may result from curvature of an original bed-parallel layer of host rock within the vein owing to differential growth of the calcite fibers from either side of the host rock-layer (Rodrigues et al., 2009; Hooker and Cartwright, 2016).

The surfaces of BPV contain domal structures, several tens of centimeters in diameter that protrude about 1 cm (0.4 in.) from the top and bottom surfaces of the BPV (Figures 4C, 5B). Inside the BPV, domal structures are characterized by an alternation of fibrous calcite and tabular host rock fragments (Ukar et al., 2017b). Domal structures are interpreted as pop-up structures bounded by thrust faults. Some are ellipsoidal with orientations that indicate east–west shortening during BPV growth, whereas others are rounded, indicating constriction on all sides, although consistently oriented north–south ribs are indicative of predominant east–west contraction. These domal structures are distinct from cone-in-cone structures as they are not the result of differential crystal growth but are formed by bed-parallel contraction and thrusting during BPV growth. It is possible that some domal structures initiated on cone-in-cone structures such as those described by Rodrigues et al. (2009). East–west shortening is compatible with the kinematics of multiple thrust faults that cut and double BPV in the area, which indicate that east–west shortening continued after BPV ceased opening (Ukar et al., 2017b). On the basis of beef fiber orientations, Rodrigues et al. (2009) also concluded that shortening occurred synchronously with BPV growth.

A transect across a 6-cm (2-in.)-thick, almost ideal, example of a BPV from the PC area shows $\delta^{18}O$ values of calcite cement ranging from approximately −9.5‰ to −10.5‰ Vienna Pee Dee Belemnite (VPDB), whereas $\delta^{13}C$ values are between approximately −0.5‰ and 1.2‰ (Weger et al., 2017). Although this variation (n = 27) is small, it indicates symmetry across the BPV, suggesting that conditions differed during growth of calcite crystals near the center and those near the outer edges. Vaca Muerta Formation host rocks surrounding this BPV have $\delta^{18}O$ values that range from about −7‰ to −8‰, slightly less negative than those of the BPV, and similar $\delta^{13}C$ values ranging from about −0.5‰ to −3‰, slightly more negative than those of the BPV (Weger et al., 2017; Figure 6). In addition, the isotopic composition of several concretions and their internal fractures showed that although the concretion fracture fill has both carbon and oxygen values similar to those of the BPV, the concretion matrix shows $\delta^{18}O$ values ranging from approximately −3.5‰ to 1‰ and $\delta^{13}C$ values between approximately +6‰ and +11‰. Stable isotopic compositions thus indicate that BPV, as well as fractures inside concretions, formed under conditions different from those during deposition and/or early diagenesis of the Vaca Muerta Formation.

Bed-Perpendicular Fractures in Outcrop

Kinematic indicators and BPV are cut by multiple sets of opening-mode bed-perpendicular fractures (Ukar

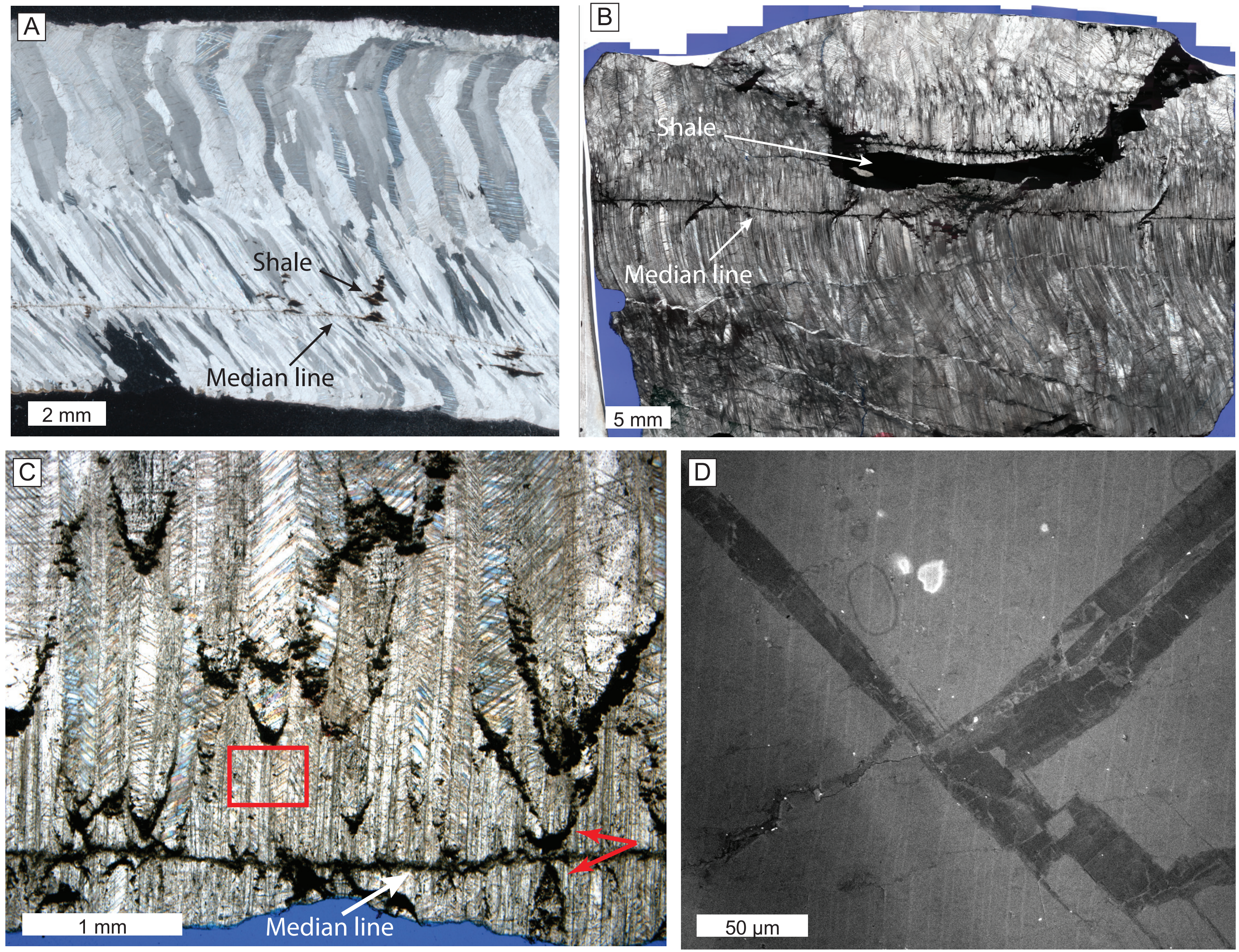

Figure 5. (A) Cross-polarized photomicrograph of BPV showing median line, curved calcite fibers, and host rock inclusions (rafts indicated as "shale") from Huncal Canyon. (B) Plane light photomicrograph of BPV from Arroyo Mulichinco showing median line, near orthogonal calcite fibers around median line and curved fibers in bottom outermost zone of BPV. Topmost part of BPV has rounded domal structure bounded by host rock (indicated as "shale") and independent median line. Both median lines in this BPV are cut by multiple mudrock-lined thrust faults. (C) Plane light photomicrograph of BPV (zone 1) showing multiple, curviplanar host rock inclusions around median line. Sense of curvature of these inclusions are opposite on both sides of median line indicating antitaxial growth of calcite fibers (arrows). Box = location of Figure 11. (D) Panchromatic SEM-CL image of dark luminescent, calcite-filled, bed-perpendicular fractures in BPV. Light luminescent, parallel bands in BPV are calcite twins. Thin section cut parallel to top wall of BPV. BPV = bed-parallel vein; SEM-CL = scanning electron microscope-based cathodoluminescence.

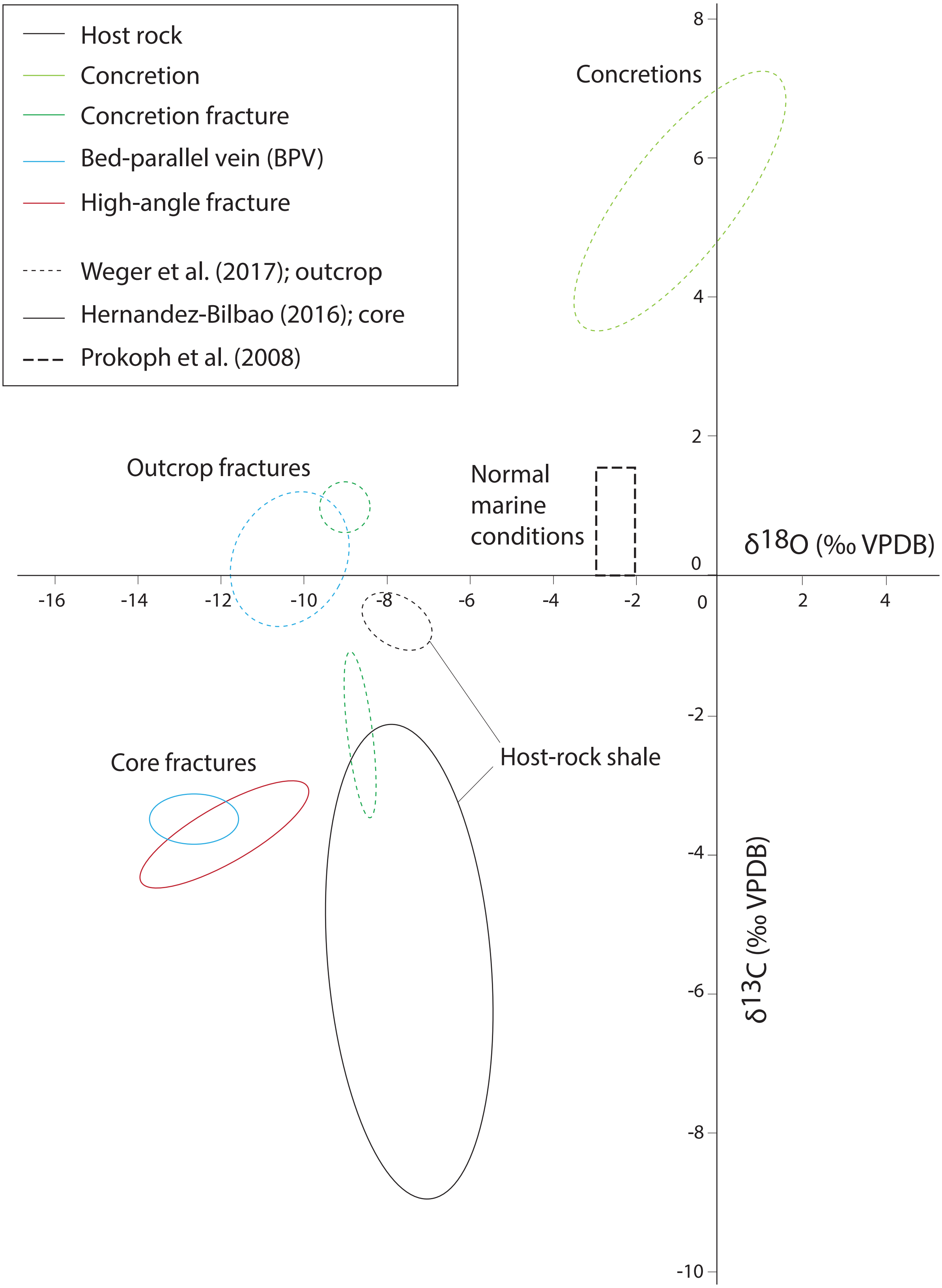

Figure 6. Stable isotope analyses of Vaca Muerta host rock calcareous mudrock, concretions, and calcite cement fill in concretion fractures, BPVs, and bed-perpendicular to high-angle fractures from Puerta Curaco outcrops (Weger et al., 2017, dashed lines) and Core 1010 in the Loma Jarillosa block (Hernandez-Bilbao, 2016, solid lines). Secular variation data from Hernandez-Bilbao (2016) after Prokoph et al. (2008). VPDB = Vienna Pee Dee Belemnite.

et al., 2017c). At Arroyo Mulichinco, bed-perpendicular fractures are in four orientations: the east–west set is the oldest, followed by the northeast–southwest and northwest–southeast sets, and the north–south set is the youngest (Figures 4C, 5D). The east–west and northwest–southeast sets are occluded by calcite cement, whereas some northeast–southwest fractures have as much as 25% residual porosity, and north–south fractures above 0.02 mm in aperture ("emergent threshold"; Laubach, 2003) contain up to 65% of fracture porosity (Figure 4C). Fractures in these, and many other, orientations also cut mudrock but are apparently barren of cement. At Puesto, east–west and north–south fractures are the most widespread in mudrock (Figure 4B), although fracture orientations are more variable than at Arroyo Mulichinco, and here the east–west set is the youngest, indicating several episodes of east–west fracture opening in the region. In scanning electron microscope-based cathodoluminescence (SEM-CL), cemented fractures of all orientations show crack-seal textures; synkinematic calcite cement indicates that fractures became cemented while fractures were actively opening. Some east–west fractures show evidence of reactivation (in opening) and contain ankerite and minor quartz cement.

Bed-perpendicular microfractures that are less than approximately 0.05 mm in aperture are absent in mudrock but cross-cut BPV and other competent layers (e.g., dolomitic marlstone; Ukar et al., 2017c). Microfractures detected using SEM-CL are as narrow as 0.0001 mm cutting BPV and 0.001 mm in a dolomitic marlstone layer. Fracture apertures measured along scanlines are as wide as 15 mm. Although mudrock on the top and bottom of BPV is highly weathered and/or eroded away, most bed-perpendicular fractures appear to be confined within the BPV. The smallest fractures terminate within these fractured layers so their height is less than the thickness of the BPV, but most terminate at the BPV boundaries so that their height is equal to the BPV thickness. This height pattern is top-bounded in the terminology of Hooker et al. (2013). For some BPV and other competent layers, some of the bed-perpendicular fractures persist into the mudrock, but terminate within a few millimeters. A few of the larger fractures (~5%) extend several tens of centimeters into the overlying and/or underlying mudrock; thus, the overall pattern is a hierarchical fracture height distribution (Hooker et al., 2013), and most fractures terminate within mudrock. At Puesto, fracture heights in mudrock range from a few centimeters to more than 1 m, although height measurements for most fractures taller than 80 cm are only minimum estimates, limited by the quality of the outcrop.

Upon closer inspection, fractures are found to be made up of multiple segments that are disconnected along their trace in plan-view, although they might be connected vertically. The segment lengths of fractures that cut competent layers range from a few centimeters to about 3 m (10 ft) even though most fractures are between 5 and 60 cm (2 and 24 in.) long. Composite fracture lengths in the competent layers can be traced for several meters but are minimum estimates limited by the extent of the outcrop. Systematically measured lengths of visible fracture segments in mudrock (macrofractures, >0.1 mm in aperture) range between 15 cm (6 in.) and 6 m (20 ft) (Ukar et al., 2017c). Composite lengths of fractures in mudrock can be traced for tens of meters.

Faults in Outcrop

Thrust faults are common in the Arroyo Mulichinco area, and they are especially abundant toward the bottom of the section, the distance between mesoscopic thrust faults ranging from 0.5 m (1.6 ft) to several tens of meters. Displacement along such faults extends from a few centimeters to several tens of centimeters, although in most cases, displacement along the fault is difficult to estimate because of erosion of the hanging wall. Toward the top of the section, thrust faults are limited to within BPV, and thrust faults do not extend from BPV into the host rock (see Ukar et al., 2017b). The consistent orientation (strike) of 12 documented thrust faults is north–south, with gentle 10° to 35° dips to the east (Ukar et al., 2017b). Slickenfibers—or aligned beef fibers within BPV—measured in the footwall of one of the thrust faults are oriented 14/079, indicating a top-to-the-west–southwest transport direction (Ukar et al., 2017b). Many thrust faults that cut BPV contain a thin layer of host rock along the fault plane, suggesting that thrusts localized along host rock inclusions.

In Puesto, most faults that cut across multiple layers are several meters to tens of meters apart, and displacements range between a few centimeters and several meters. Fault planes are generally oriented north–south to northeast–southwest and dip 10° to 20° to the northwest. Although most faults show reverse movement, about 10% exhibit an apparent, normal movement. Most fault planes are barren of cement, although some have as much as 25-cm (10-in.)-thick calcite cement. An apparent fault visible at the top of a cliff exposure contains calcite infill approximately 0.5 m (1.6 ft) wide. Carbonate cement with similar characteristics and orientation protrudes from the cliffside, but the relationship to faults is undetermined owing to the poor quality of the outcrop around the resistant cement.

FRACTURES IN THE SUBSURFACE

The most common types of fractures observed in the cores are BPV and low-angle fractures (Figure 7A–C), compacted vertical fractures (Figure 7D), and bedding–oblique-to-perpendicular fractures with planar walls (Figure 7E–F). In some cores, such as in cores E and SC, BPV constitute about 95% of the fractures (de Barrio et al., 2018), probably because these cores are vertical and spacing of high-angle fractures is larger than the width of the core (see "Fracture Abundance" section), rendering them difficult to capture. Because many of these fractures are below the resolution of borehole images and seismic tools, they are observable only at smaller scales through core description and microscopy methods.

In most of the cores we analyzed, deformed vertical fractures (ptygmatic fractures) (oldest) are cut by BPV, which in turn are cut by planar, bed-perpendicular fractures (youngest). In some cases, however, such as in SC cores, BPV cut bed-perpendicular fractures, indicating that some bed-perpendicular fractures predate BPV. Although the rabbled nature of outcrops might have obscured ptygmatic fractures, this type of fractures were not observed in outcrop.

Ptygmatic Veins

Early ptygmatic veins terminate at lithological changes or display differential compaction within different lithologies (Figures 7E, 8A). Ptygmatic veins may be branching, and most are infilled by blocky calcite cement, although in some cases, they are filled with quartz/gypsum and a later-opening increment is filled with carbonate cement (siderite). Cementation of these early fractures predates final compaction.

Bed-Parallel and Low-Angle Fractures in Core

In general, BPV in core are narrower than those observed in outcrop; the widest BPV in core are only between 1.5 and 2 cm (0.6 and 0.8 in.) wide in contrast to more than 10 cm-thick BPV in outcrop. Many BPV are localized at lithological changes or carbonate concretions as in outcrops (Figure 4D), and some nucleate on fossils. Wang (2016) reported that about 75% of clear, mechanical interfaces were associated with BPV development in core. BPV may be present as isolated microfractures (apertures <0.1 mm) or as part of a complex fracture network or zone, and in some cases form en-echelon arrays or extensive relay zones (releasing stepovers) (Figure 7B). Some BPV appear to be buckled and occur together with subvertical stylolites, both indicating a tectonic shortening event (Figure 7C).

As in outcrop, BPV in core generally contain fibrous calcite cement and host rock inclusions (Figure 8B–G). Wide BPV are infilled by curved, fibrous calcite cement, indicating two to three opening stages probably during bed-parallel shear. In a few cases, BPV are filled with blocky calcite rather than fibrous calcite cement, and thick BPV (>~3–4 mm) may preserve porosity (<~10%, Core E; Figure 8F). Some BPV are associated with low-angle fractures, which may be contemporaneous with or postdate BPV (Figure 7A). Such low-angle fractures are as narrow as 0.3 mm in aperture and are filled with blocky calcite cement. Similar to BPV, some low-angle fractures have elongated, blocky-to-fibrous calcite cement, indicating shear. Domal kinematic indicators identified in outcrop are small enough to be captured in core and were identified south of the field study area in cores B and C (see Ukar et al., 2017b).

In Core 1010, $\delta^{18}O$ values of calcite cement within BPV range from −11.69‰ to −13.33‰ VPDB with an average $\delta^{18}O$ of −12.42‰ VPDB. The $\delta^{18}O$ values of lower Vaca Muerta host rock range from −6.76‰ to −13.59‰ VPDB, with an average $\delta^{18}O$ of −8.24‰ VPDB (Hernandez-Bilbao, 2016; Figure 6). The $\delta^{13}C$ values range between −3.58‰ and −3.70‰ VPDB, with an average of −3.60‰ VPDB, whereas $\delta^{13}C$ values of the host rock range from −2.48‰ to −8.77‰ VPDB, with an average $\delta^{13}C$ value of −4.28‰ VPDB. Calcite cement in BPV is bright orange luminescent (Figure 8G) consistent with precipitation under deep burial conditions from pore fluids rich in Mn and Fe (Hiatt and Pufhal, 2014).

Bed-Perpendicular Fractures in the Subsurface

Fracture orientations in the subsurface were established on the basis of resistivity image logs or Formation Microimager Images (FMI). In cores dominated by mudrock, the combination of overpressure and coring operations may lead to generation of subtle-to-intense induced fractures, which were excluded from the natural fracture data sets. The strike of bed-oblique to bed-perpendicular natural fractures in the studied wells is mainly east–west, northeast–southwest, and northwest–southeast, and dip is from 71° to 90° to bedding (Figure 9). In Core 1010, most fractures strike east–west and dip from 71° to 77° to the north. Similarly, bed-perpendicular fractures in Sierra Chata dip between 70° and 90° and strike mainly east-northeast–west-southwest, a few fractures being oriented north-northeast–south-southwest, east–west,

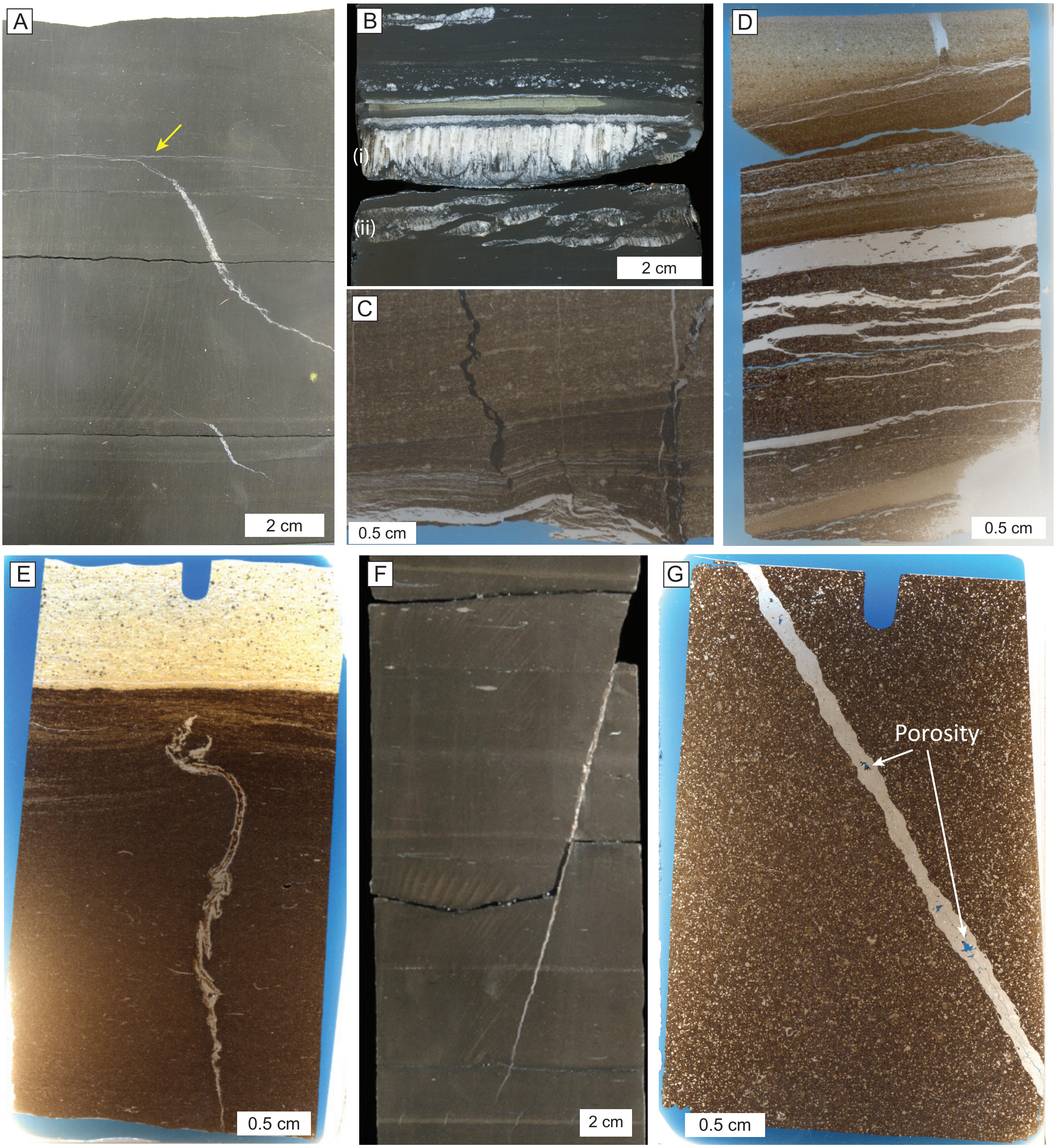

Figure 7. Photographs of fractures in core. (A) Oblique–to–low-angle fracture terminating against and joining narrow BPV in Core 1010. (B) Bed-parallel fractures (BPV) in Core SC, natural light. (i) BPV showing U-shaped host rock fragment arrays intercalated within calcite fibers (cone-in-cone structures). (ii) En-echelon BPV (de Barrio et al., 2018). (C) Thin section of bed-perpendicular stylolites and calcite-filled fractures terminating against deformed, calcite-filled BPV in Core B. (D) Thin section of cluster of calcite-filled BPV in Core B. (E) Thin section of ptygmatic fracture showing strong lithological control in Core C. (F) Calcite-filled, bed-subperpendicular fracture in Core 1010. (G) Calcite-filled fracture at high angle to bedding showing approximately 10%–15% residual fracture pore space in Core C. BPV = bed-parallel vein.

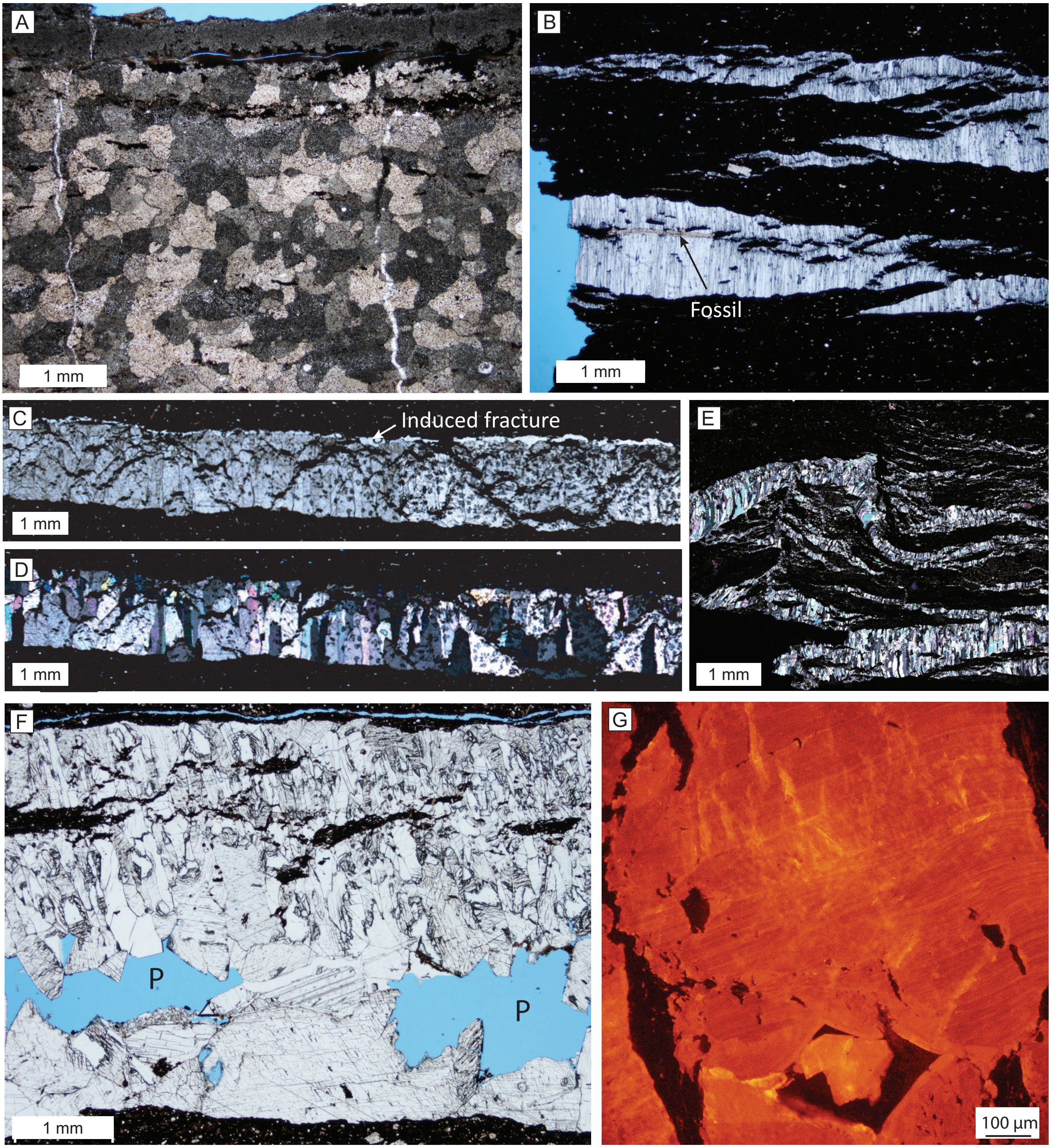

Figure 8. (A) Cross-polarized photomicrograph of deformed, calcite-filled, bed-perpendicular fractures terminating at lithological change in Core E. (B) Plane light photomicrograph of fibrous calcite-filled BPV in Core E, showing complex textures and multiple muddy inclusions from the host rock. Part of median line of bottom BPV is a fossil. (C) Plane light photomosaic of BPV in Core 1010 showing multiple curviplanar host rock inclusions. Sample split along contact between fracture and host rock. (D) Cross-polarized image of (C). (E) Cross-polarized image of deformed BPV with fibrous texture, as seen in Figure 7C. (F) BPV in Core E with fibrous calcite and euhedral crystal terminations indicating porosity (P) preserved in center of the BPV is primary. (G) Optical-CL image of BPV in (C), (D) showing bright orange luminescence.

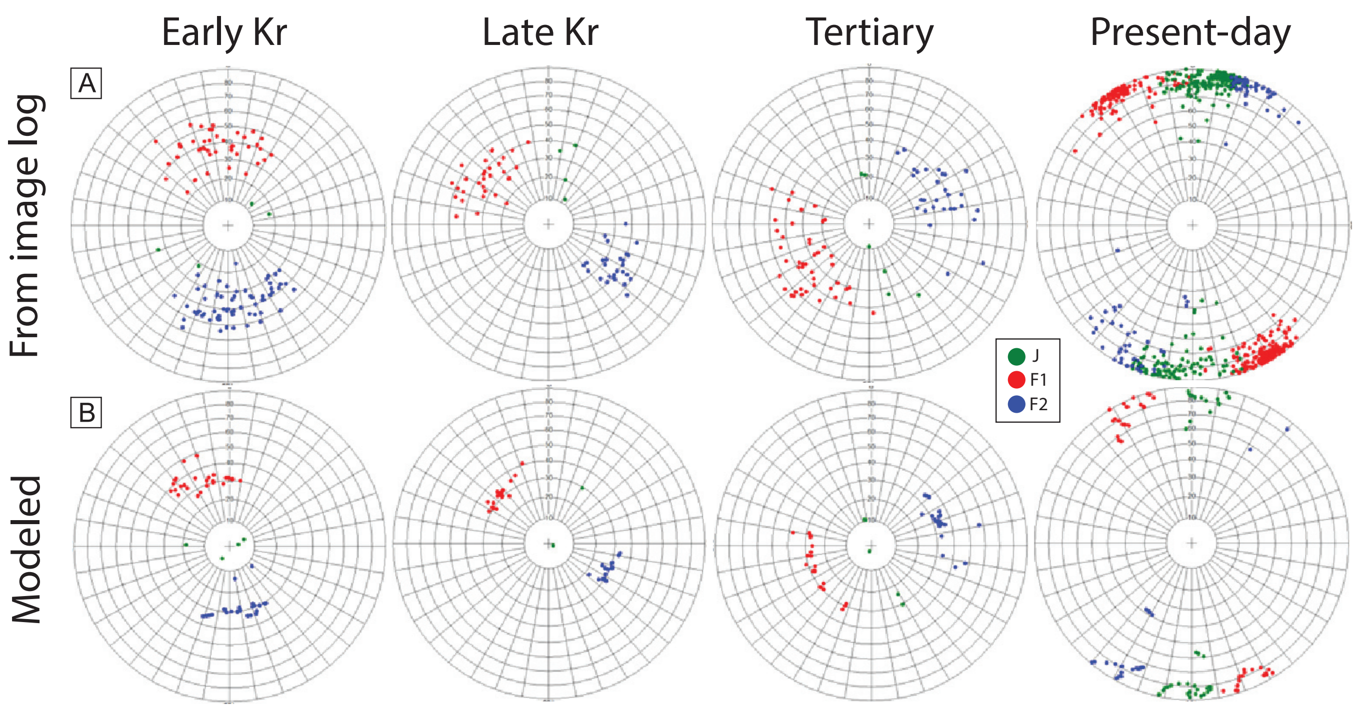

Figure 9. (A) Poles to fracture planes in subsurface as imaged using image logs and (B) as modeled. Ages of imaged fractures assigned on the basis of modeling results. J = joint; F_1 and F_2 = conjugate shear fractures.

and north–south. We note that many more fractures are present in core that were not imaged by image logs, either because their size is below the detection limit of this technique or because the resistivity contrast between host rock and fracture was too low.

Bed-perpendicular microfractures as narrow as 0.0004 mm are present cutting some competent layers (e.g., altered tuff) in core, but they are absent cutting BPV, and microfractures narrower than 0.03 mm are absent in mudrock. The tallest high-angle fractures measured in core are upward of 1 m, but these are minimum height estimates because fractures continue beyond the core.

Bed-perpendicular fractures are generally infilled by blocky calcite and host rock inclusions, and some show multiple opening events (Figure 7F, G). Bed-perpendicular fractures contain bitumen in some cores, and residual fracture porosity in fractures wider than about 0.1 mm (emergent threshold for core) may be as much as 25% to 40% but is more commonly 5% to 10%. In contrast, microfractures less than about 0.1 mm in aperture are infilled completely by cement. Minor cements present in some bed-perpendicular fractures include gypsum, siderite, pyrite, and quartz. A few bed-perpendicular fractures are infilled by fibrous calcite cement, although fibrous cements are not the norm. In bed-perpendicular fractures that cut competent, recrystallized tuff layers, crack-seal textures are widespread.

Bed-perpendicular fractures cut tectonic stylolites, which in turn are contemporaneous with or postdate BPV (Figure 7C). In some cores, anastomosing, irregular, low-angle fractures filled with blocky calcite terminate against or connect with bed-perpendicular fractures also filled with blocky calcite, indicating that low-angle fractures postdate or are contemporaneous with bed-perpendicular fractures. Cores therefore show evidence of multiple stages of low-angle fracture formation, and some bed-perpendicular fractures show evidence of reactivation in shear, especially those cutting competent layers such as BPV and recrystallized tuff (Figure 8A).

The $\delta^{18}O$ values for calcite within bed-perpendicular fractures in Core 1010 range from −10.09‰ to −13.09‰ VPDB, with an average of −12.29‰ VPDB. The $\delta^{13}C$ values for calcite cements range from −3.10‰ to −4.00‰ VPDB, with an average of −3.79% VPDB (Hernandez-Bilbao, 2016; Figure 6). These isotopic values, although similar to those for calcite in BPV, are more depleted in ^{18}O than those of the Vaca Muerta Formation host rock. Bright orange luminescence of calcite cement in these fractures is also consistent with precipitation under deep burial conditions (Hiatt and Pufhal, 2014).

Faults in the Subsurface

Poly-episodic deformation in the Neuquén Basin resulted in several events of fault formation and reactivation (see Marchal et al., 2020, this Memoir). The present-day stress regime, as indicated by borehole breakouts within the Vaca Muerta Formation throughout most of the Neuquén Basin, is strike slip and decreases in stress anisotropy to the east away from the influence of the Andes and into the thick sediment package of the embayment (Garcia et al., 2013; Varela et al., 2020, this Memoir). The main faults in the Vaca Muerta–Quintuco System are as follows: (1) northwest–southeast, east-northeast–west-southwest, north-northeast–south-southwest, east–west, and radial normal faults, (2) east–west, north–south, northeast–southwest, and circular reverse faults, (3) north-northwest–south-southeast and north-northeast–south-southwest thrust faults, and (4) east-northeast–west-southwest strike-slip faults (Marchal et al., 2020, this Memoir).

Normal faults formed mainly during the Late Triassic to Early Jurassic rifting that caused reactivation of basement faults. A classical horst-and-graben system developed along the boundaries of the embayment, whereas an en-echelon system developed in the eastern part of the embayment as a result of this deformation (Cristallini et al., 2009). Oblique reverse faults are oriented mainly east–west around the Huincul High, and north–south faults are prominent at the front of the fold-and-thrust belt on the western margin of the basin. Low-angle thrust faults are oriented north-northwest–south-southeast around the Añelo Trough whereas they trend north-northeast–south-southwest in the western part of the basin. Finally, pure northeast–southwest strike-slip faults are present to the west of the Añelo Trough (Gangui and Grausem, 2014; Marchal et al., 2020, this Memoir).

In the Loma Campana and Loma Jarillosa areas, a main series of faults are oriented north-northwest–south-southeast, whereas in the nearby Huincul High faults strike west-northwest–east-southeast (Figures 1A, 3). The main fracture strike in Loma Jarillosa is nearly perpendicular to the strike of the main faults in this area of the embayment, whereas faults in Sierra Chata, on the eastern flank of the Chihuidos High, are parallel to the east-northeast–west-southwest set and are basement-reactivated faults that affected the sedimentary cover. According to our structural interpretation (Figure 3B), fault activity that affected the Vaca Muerta Formation in the Loma Campana area, with displacements of up to several tens of meters, occurred in Early Cretaceous, Late Cretaceous, and Tertiary. These orientations contrast with the north–south general trend of faults in the studied outcrops within the Agrio fold-and-thrust belt (Figure 2).

FRACTURE ABUNDANCE

Fracture Abundance in Outcrop

Rodrigues et al. (2009) and Weger et al. (2019) measured the abundance of BPV as a percentage of rock volume and established that the Loncopué and PC sections contains about 10% and more than 4% BPV, respectively, the highest measured in our study areas.

For abundance and size distributions of fractures over a range of scales to be compared, opening-displacement data are expressed as "cumulative frequency," the cumulative number (N) or rank of fractures sorted by aperture size and normalized by scanline length (L). In cumulative frequency versus aperture log-log plots, the best-fit equation for a straight line is a power law, $y = ax–b$, in which x is aperture, y is cumulative frequency, a is intensity of fracture distribution, and b is slope (Marrett et al., 1999).

In such graphs, bed-perpendicular fractures commonly show power-law aperture size distributions irrespective of host rock lithology (e.g., Marrett et al., 1999). Ukar et al. (2017c) found power-law aperture size distributions for bed-perpendicular fractures in the folded Loncopué outcrops. There, the north–south, bed-perpendicular set shows lower intensities than does the east–west set. Fracture frequencies for 0.1 mm and wider macrofractures range from 20 to 35 fractures/m for east–west fractures at Arroyo Mulichinco and from 5.3 to 7.0 fractures/m at Puesto, whereas north–south fractures away from faults are 5.1 fractures/m and 4.8 fractures/m, respectively. Similar macrofracture frequencies were measured in narrow (a few tens of centimeters), competent BPV and altered tuff layers and in thicker (several meters) mudrock units, but no consistent bed thickness-to-spacing relationship was found. Also, nonreactivated microfractures that cut BPV were found to be good predictors of macrofracture abundances in mudrock. Normalized correlation count analysis (NCC, Marrett et al., 2018) of the spatial arrangement of bed-perpendicular fractures in the BPV at Arroyo Mulichinco indicates that whereas microfractures are arranged in clusters with a fractal distribution within clusters, macrofractures in BPV are mostly regularly spaced (Figure 4C). Macrofractures in mudrock at Puesto are clustered around faults. Near north–south-striking faults at Puesto, north–south fracture frequency in the mudrock is an order of magnitude higher than away from faults

(38 fractures/m), suggesting a fault-influenced mechanism for the growth of these fractures.

Although in detail the spatial arrangement is different at different scales, for regularly spaced macrofractures, average spacing is a useful measure. Size frequency can be inverted to yield average spacing of fractures of a given size or larger (Ortega et al., 2006; Hooker et al., 2009, 2014). Average fracture spacings of east–west fractures (0.1 mm and wider) are from 0.028 to 0.049 m at Arroyo Mulichinco and between 0.144 and 0.187 m at Puesto, whereas north–south fractures are 0.195 m and 0.209 m, respectively, and 0.026 m near faults (Ukar et al., 2017c).

Few systematic studies of BPV population size distributions exist, but Wang (2016) found that 9 out of 10 populations of BPV, including three outcrop (Arroyo Mulichinco) and five core data sets from the Vaca Muerta, show negative exponential aperture size distributions. The difference in aperture size distribution function (compared to the power-law function for bed-perpendicular fractures) is possibly linked to the different configuration of stress, which for BPV commonly includes contemporaneous compression (Rodrigues et al., 2009; Ukar et al., 2017b; Zanella et al., 2020) and the impact of bed-parallel weakness on BPV development.

Fracture Abundance in Core

In Core 1010, average intensity of BPV as measured along a 1-D scanline following the core axis is 8.6 fractures/m (~0.116 m spacing). Two distinct intervals have higher BPV intensities of 27 fractures/m (0.055 m spacing) and 18 fractures/m (0.037 m spacing) between 3103.40 and 3104.40 m (10,181.79 and 10,185.04 ft) and between 3099.00 and 3100.00 m (10,167.32 and 10,170.60 ft) depth, respectively. These intervals have a high TOC percentage between 2.47 wt. % and 9.57 wt. %. Intensity of BPV in Sierra Chata ranges from 1.15 to 7.1 fractures/m where fracture intensities increase with TOC and hydrocarbon saturation (Marchal et al., 2016).

In Sierra Chata, intensity of filled, bedding-oblique macrofractures as measured on image logs is 0.365 fractures/m (2.74 m [8.99 ft] spacing), fracture intensity increasing within carbonate-rich intervals and closer to faults (up to 17 fractures/m). In core, bed-perpendicular microfractures are absent in mudrock and in thin BPV, and macrofracture spacing is too large to permit a scaling analysis similar to that performed for outcrop. Two recrystallized tuff layers from Core C, however, contain bed-perpendicular microfractures that we used for scaling analysis (Figure 10; see Ukar et al., 2017c for methodology). Fracture frequencies for 0.1 mm and wider macrofractures here range from 15 to 146 fractures/m, and average spacings for these fractures are between 0.007 and 0.066 m (Table 1). These fracture frequencies and spacings are similar to those measured in outcrop (Figure 10). Average fracture spacings, however, must be used with care here; they are applicable for regularly spaced macrofractures but not for clustered microfractures.

Bed-Parallel Veins Abundance and TOC

The Vaca Muerta Formation contains intervals with high TOC, which in the subsurface is up to 20 wt. % but averages 5 wt. % (Hernandez-Bilbao, 2016; Tenaglia et al., 2017; Minisini et al., 2020, this Memoir). In outcrop, TOC varies from less than 0.1 wt. % to 9.7 wt. % (Tenaglia et al., 2017). TOC increases toward maximum flooding surfaces and decreases in more regressive parts. In the "Fracture Abundance in Core" section, we indicated that Marchal et al. (2016) documented that fracture intensities increase with TOC and hydrocarbon saturation. We now provide more information on reported relations between BPV abundance, thickness, and TOC.

In four cores distributed from the eastern border of the embayment to the Chihuido High, Palacio et al. (2018) found a direct relationship between BPV thickness and distance to the Agrio fold-and-thrust belt. They also reported an increase in BPV thickness with hydrocarbon maturity, from southeast to northwest of the basin. This relationship is well illustrated over the embayment area, where thicker BVP are present from the oil window to the gas window (Palacio et al., 2018). Moreover, BPV thickness appears to be at least partly related to TOC content because thicker BPV are present in the lower enriched section (OVM1 *sensu* Domínguez et al., 2016) than in the upper enriched section (OVM4 *sensu* Domínguez et al., 2016; de Barrio et al., 2018). Within the same maturity window, BPV abundance generally decreases from base to top, following the decreasing trend of TOC content (Al Dulhailan and Sonnenberg, 2015; Domínguez et al., 2016; Hernandez-Bilbao, 2016; Marchal et al., 2016; Palacio et al., 2018). This general trend might reflect higher overpressure at the base or control of TOC on BPV development although the two could be linked through a formation mechanism of increased fluid overpressure resulting from hydrocarbon generation in high-TOC mudrocks. Wang (2016) found a correlation between TOC and BPV intensity in some Vaca Muerta cores (B and D), but not in others (Core F), finding instead that interfaces between layers with contrasting mechanical properties have a stronger control over location of BPV than TOC content. These interfaces act as weak planes for BPV initiation; the number of interfaces within a given section might also control BPV abundance. Which of these factors has the most influence on BPV abundance, and whether there is an additional control on thickness, is not clear.

As in core, in outcrop, BPV abundance decreases upsection at Arroyo Huncal, this decrease corresponding partly to an overall upward decrease in TOC (Larmier et al., 2018). Weger et al. (2019) also found a weak relation between TOC content and BPV abundance in the PC area ($R = 0.10$, $p = 0.003$). Qualitative observation of the abundance logs suggests a weak qualitative link between the amount of tuff and presence of TOC, although neither is quantitatively correlative to the presence of BPV (Weger et al., 2019).

FLUID INCLUSION AND CLUMPED ISOTOPE THERMOMETRY

Outcrop Thermometry

Primary, two-phase, liquid-rich, aqueous fluid inclusions in BPV calcite from Arroyo Mulichinco show homogenization temperatures (T_h) (to liquid) that range from about 175°C to 210°C (347°F to 410°F), and fluid salinities of about 15% NaCl equivalent, with no significant variation of either among successive zones (Ukar et al., 2017a; Figure 11). Initial ice-melting temperatures indicate that the fluid present in these inclusions contains $CaCl_2$ ($\pm MgCl_2$) as well as NaCl. Moreover, T_h of fluid inclusions in bed-perpendicular fractures ranges between about 146°C and 161°C (295°F and 322°F) for the east–west set, from 143°C to 154°C (289°F to 309°F) for the northwest–southeast set, and from 144°C to 156°C (291°F to 313°F) for the north–south fracture set. The northwest–southeast set did not contain fluid inclusions appropriate for microthermometric analysis.

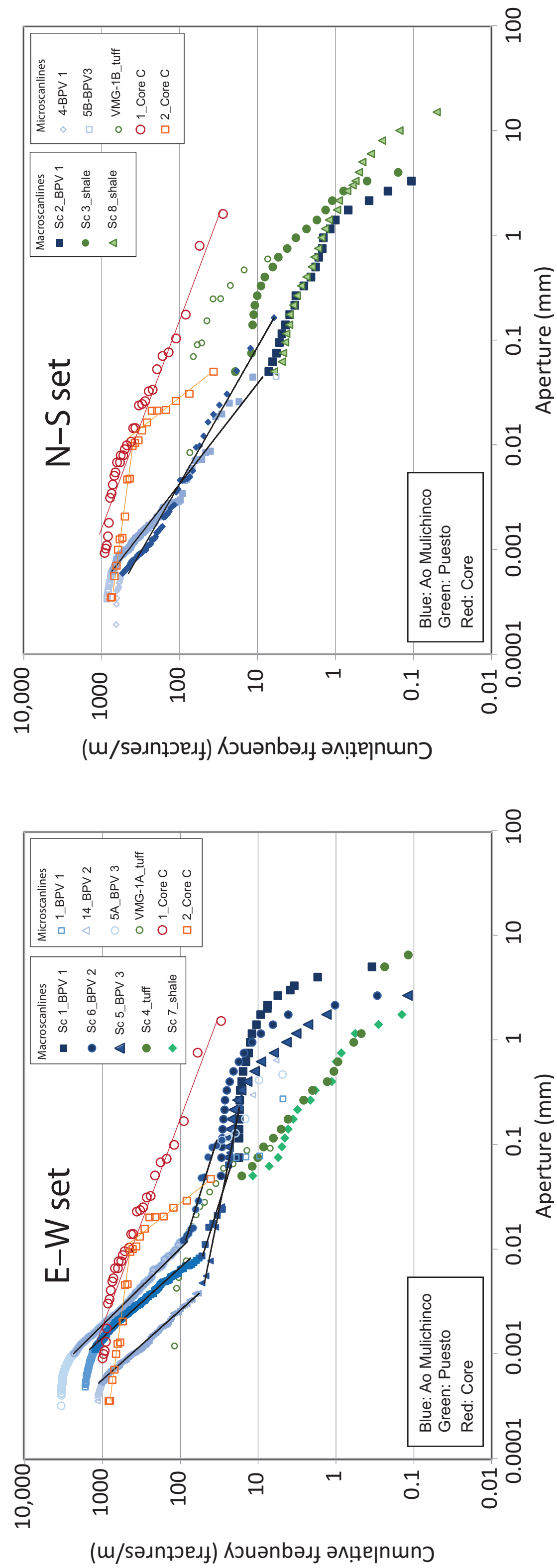

Figure 10. Aperture versus cumulative frequency log-log plots of macrofractures measured along scanlines in the field and microfractures measured along microscanlines using SEM-CL images. Fracture abundance from two core samples (Core C) compared with outcrop data for sets 1 (east–west) and 4 (north–south), as reported by Ukar et al. (2017b). Orientation of fractures in core unknown. Note that narrow and wide microfractures in sample 2_core C follow two distinct power laws with different slopes. BPV = bed-parallel veins; SEM-CL = scanning electron microscope-based cathodoluminescence; tuff = altered/recrystallized volcaniclastic layer; shale = mudrock.

Table 1. Microscanline properties and microfracture frequency and spacing calculations.

Microscanline	Lithology	Layer thickness (cm)	Scanline length (cm)	Number of fractures	Distribution	Equation	R^2	Frequency (m^{-1}) 0.01 mm	Frequency (m^{-1}) 0.1 mm	Frequency (m^{-1}) 1 mm	Spacing (m) 0.01 mm	Spacing (m) 0.1 mm	Spacing (m) 1 mm
1_Core C	Recrystallized tuff	10	3	34	Power-law	$y = 48.8x^{-0.476}$	0.957	437	146	49	0.0023	0.0068	0.0204
2_Core C narrow	Recrystallized tuff	4	5	11	Power-law	$y = 168.7x^{-0.193}$	0.9784	410			0.0024		
2_Core C wide	Recrystallized tuff	4	5	10	Power-law	$y = 0.5x^{-1.487}$	0.9345		15	1		0.0667	1.0000

Most of the calcite cement analyzed in this study precipitated during fracture opening (synkinematic), so fluid inclusion temperatures from these cements provide an estimate of the temperature and composition of the fluid during fracture opening and concurrent cementation. All fractures contain coexisting aqueous fluid and hydrocarbon gas inclusions within the same fluid inclusion assemblage (FIA) (Fall and Bodnar, 2018); therefore, T_h of the inclusions represents true trapping temperature (Goldstein and Reynolds, 1994). Hydrocarbon gas inclusions in both BPV and bed-perpendicular fractures are liquid at room temperature and homogenize at about 75°C, indicating that the hydrocarbon is primarily methane dominated, possibly containing other gas phases such as CO_2 and ethane and/or propane. The presence of probably low concentrations of CO_2 in the gas inclusions was confirmed using Raman microspectrometry (Fall et al., unpublished data).

Aqueous fluid inclusions are saturated with methane at trapping temperature, as indicated by coexisting gas inclusions within the same FIA, and their methane concentration ranges from about 4500 to 5500 ppm. These concentrations correspond to trapping pressures (Becker et al., 2010; Fall et al., 2015) ranging from about 180 MPa near the median line to about 80 MPa in the outer zones of BPV (Fall et al., unpublished data). Pressures of fluid inclusions trapped in the innermost zones of BPV are the highest, showing near–lithostatic-to-lithostatic pressures, indicating overpressure conditions during the early stages of bed-parallel fracture opening and cementation of BPV. Pressure estimates potentially indicate the actual pore fluid pressure required to overcome lithostatic overburden stress and to initiate bed-parallel fracturing aided by bed-parallel contraction. The outer, later-formed zones of BPV show lower pressures but indicate that overpressure conditions continued during later stages of fracture opening and cementation.

Another method that allows estimation of temperature conditions during mineral precipitation is clumped isotope analysis (Ghosh et al., 2006). This technique is based on a thermodynamic force that is driven by increased stability in molecules containing bonds between heavier, rare isotopes (^{13}C, ^{18}O) as temperature decreases. Accurate measurement of the abundance of these bonds in carbonate-derived CO_2 gas (Δ_{47}) relative to the abundance that would be found if all molecules followed a stochastic distribution allows the formation temperature of a carbonate material to be determined, as this ratio is strictly controlled by temperature and independent of the composition of the precipitating fluid (Ghosh et al., 2006). Clumped isotope temperatures can then be used in conjunction

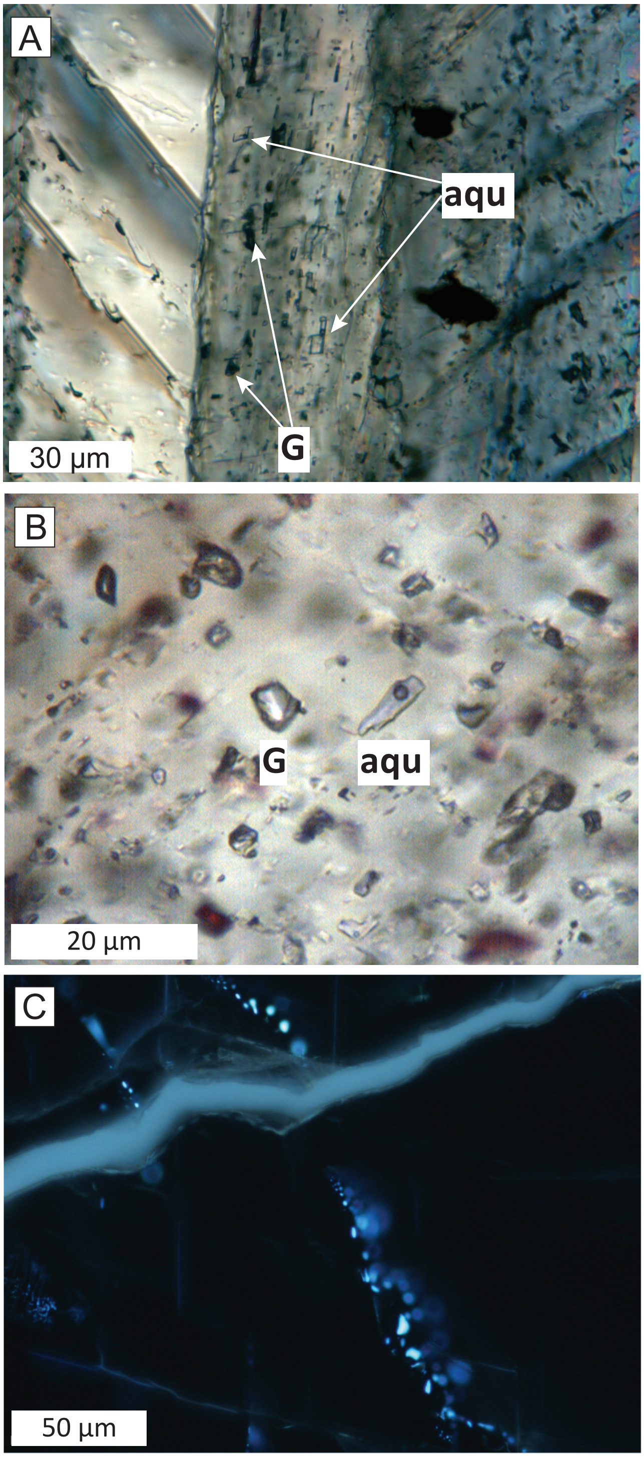

Figure 11. (A, B) Plane light photomicrographs of calcite in innermost part of a BPV in outcrop (Figure 5C), showing coexisting primary, two-phase aqueous (aqu) and single-phase gas (G) inclusions. (C) Trails of secondary blue-fluorescent oil inclusions in a BPV from Core E. aqu = aqueous; BPV = bed-parallel vein.

with $\delta^{18}O$ carbonate fluid calibrations to determine the $\delta^{18}O$ composition of the precipitating fluid.

Weger et al. (2019) used clumped isotope analysis to constrain both the temperature at which calcite cement in BPV, surrounding host rock, early diagenetic concretions, and fractures within concretions formed as well as the isotopic composition of fluids present during sediment deposition and cement precipitation in Vaca Muerta Formation outcrops. Clumped isotope temperatures determined by Weger et al. (2019) for BPV in the SdlVM, Loncopué, YdT, and PC areas indicate formation temperatures of BPV that range between 140°C and 195°C (284°F and 383°F). Temperatures in the PC area are dominant around 180°C (356°F) (160°C [320°F] when all measured BPV samples are considered). Vaca Muerta Formation host rock above and below (0.5 m, 5 m, and 10 m [1.6, 16, and 33 ft]) the BPV in PC show significantly lower temperatures, ranging from about 120°C to 150°C (248°F to 302°F).

Core Sample Fluid Inclusions

Fractures of all types in all cores analyzed lack primary, two-phase fluid inclusions suitable for microthermometry primarily because of the small size of the few observed inclusions. A few trails of secondary, oil inclusions were observed in calcite cements in bed-perpendicular fractures that are clear under transmitted light and show a light blue fluorescence under UV light (Figure 11). The composition of the oil in the inclusions is unknown. However, the light blue fluorescence of the oil inclusions indicates that the inclusions trapped a light, volatile oil. The oil inclusions have variable liquid-to-vapor ratios, and both single- and two-phase inclusions have been observed within the same FIAs. The secondary nature of the inclusions indicates that oil was present in the microfractures after primary fracture cementation ceased. To date, no clumped isotope data have been reported for fractures in cores of the Vaca Muerta Formation.

MODELING FRACTURES IN LOMA CAMPANA BLOCK: AN EXAMPLE

For a subarea of the Neuquén Basin, an example of how fracture data can be used to create a DFN model can now be presented. The approach is to first make a geomechanical model of fracturing through time that is based on the tectonic framework of the area using the large structures as guides and image logs, cores, and outcrop data as constraints. Without appropriate fluid inclusions for microthermometry or cross-cutting relationships of oriented fractures in core, fracture timing was determined on the basis of a tectonic model. Using 3-D seismic data and structural reconstruction of the western margin of South America from the literature, we inferred four main deformational events for the Loma Campana block (Figure 12) during Early Cretaceous, Late Cretaceous, Tertiary, and present-day epochs. These four main tectonic events are considered responsible for development of the present-day natural-fracture network. The orientation of the principal maximum stress was horizontal during these events (Mosquera and Ramos, 2005).

Tectonic Model Construction

Fracture orientations and distribution across the studied area were constrained using 3-D geomechanical modeling that takes into account past remote stresses and tectonic regimes following the method of Maerten et al. (2016) and Hryb et al. (2018). Local main stress vectors (s_1, s_2, s_3) that result from the interaction between remote stresses and mapped subsurface faults (Figure 3) were calculated for each cell of the model. The fracture criteria applied were based on Andersonian fault theory, in which three main fracture types may be developed in a rock under stress (Anderson, 1905; reprinted 2012)—joints (J) perpendicular to s_3, and two conjugate shear fracture planes (F_1 and F_2) intersecting at s_2 having a theoretical friction angle of 30° about s_1. The s_3 magnitude for joints and maximum Coulomb shear stress (MCSS) for shear fractures were used as intensity drivers to calculate intensity through the modeled volume (“intensity tendency”). To account for uncertainties in paleo-stress orientations, we considered several stress vector orientations and stress regime scenarios for each tectonic event (e.g., Early Kr N310, Early Kr N320) in an iterative process. Orientations of natural fractures identified in image logs (Figure 9) were compared with those modeled for each scenario using internally developed software (following Hryb and Lopez, 2015), and the fractures in the image logs were then assigned to the event and type that best matched their orientation.

Intensity tendency grids were calculated on the basis of the relation between fault orientations and remote stresses as established for each deformational event (Figure 13A). The total P32 fracture intensity (fracture surface area/rock volume; Dershowitz and Herda, 1992) for all fracture types across the Loma Campana area was modeled by calibrating 3-D intensity grids for each deformation event and fracture type using image logs. The P10 fracture intensity was measured along 1-D scanlines in image logs (P10, number of fractures/m). As P32 is challenging to measure, P10 was a proxy for P32 for the construction of our models; for each fracture set and each mechanical unit, P32 was calculated from the measured P10 and fracture orientation. This P32 fracture intensity was then plotted against P32 calculated from the fracture intensity driver (s_3 or MCSS; Figure 13B). The relationship from these cross plots allowed for calibration of 3-D fracture intensity grids (Figure 13C) and the final P32 fracture intensity distribution model (Figure 13D).

Tectonic Model Results

Fracture orientations modeled on the basis of the stress configurations described earlier are approximately east–west to east-northeast shear fractures (F_1 and F_2) in the Lower Cretaceous, northeast–southwest joints (J) in the Upper Cretaceous, northwest–southeast in the Tertiary, and east–west to east-northeast in the present day (Figure 12). Modeled orientations offer a good representation of fracture orientations observed in image logs for the Loma Campana block (Figure 9). Modeled fracture intensity distribution 3-D grids show that fracture intensities (P32) for each tectonic event depend on mechanical stratigraphy and fault orientations (Figure 13).

DFN Model Construction

We constructed DFN models that show representations of natural fracture planes in the subsurface using Petrel™ and internally developed software following the general parameters shown in Table 2 for the Loma Campana area. To populate DFN models, we used 3-D grids of fracture orientation and intensity (P32) obtained from tectonic models as described earlier. We did not observe a consistent fracture stratigraphy in outcrop or cores, so we had no basis for constructing a fracture stratigraphy within the mudrock facies of the DFN and did not do so. Because BPV are controlled by many factors, a systematic, statistical correlation between fracture intensity and depth, TOC, overpressure, density, or other attributes could not be established. Therefore, only fractures oriented at a high angle to bedding were considered by the model.

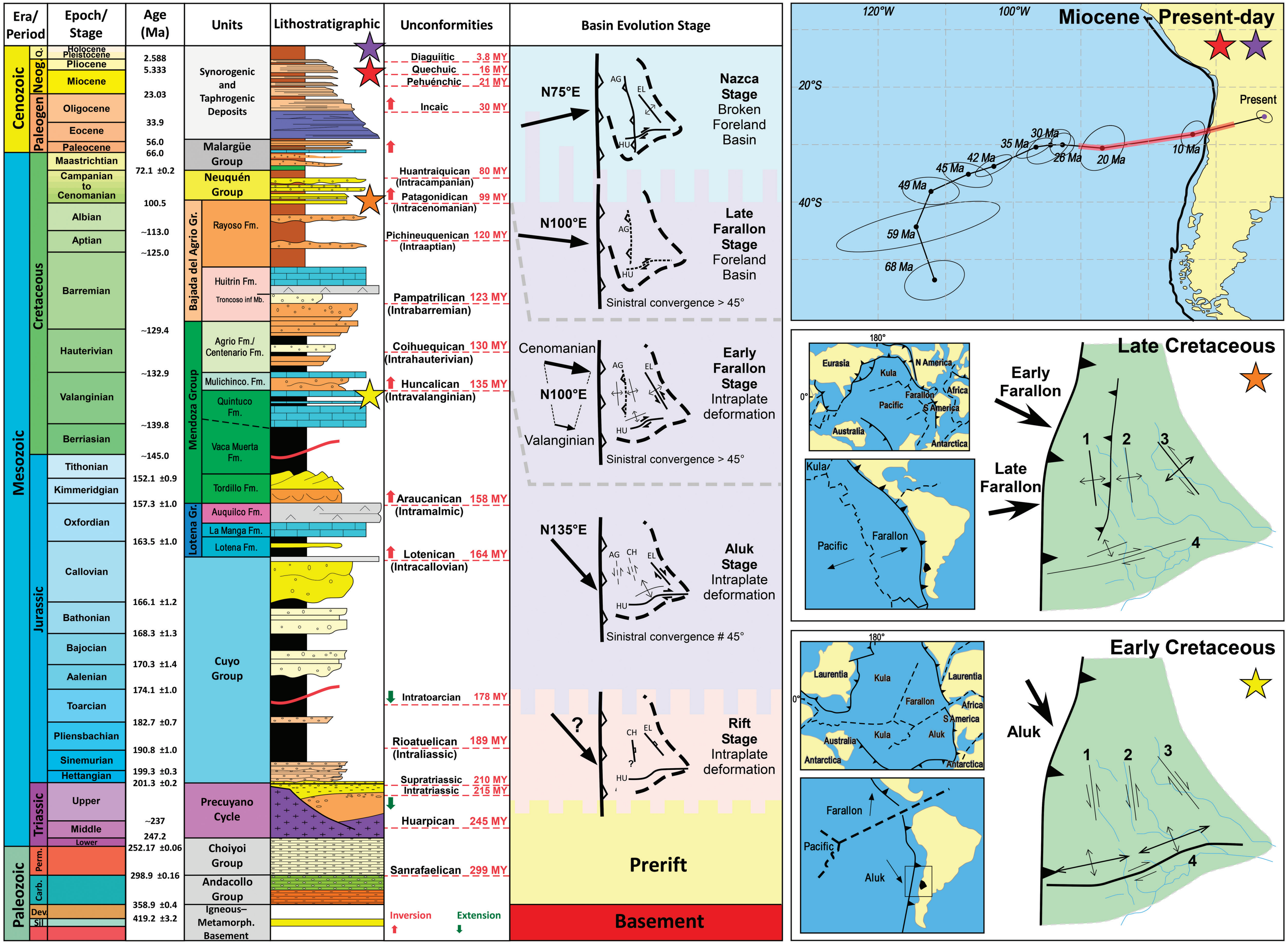

Figure 12. Main tectonic events used in the construction of our tectonic model, as defined by changes in stress direction over time. Modified from Pardo-Casas and Molnar (1987) and Mosquera and Ramos (2005).

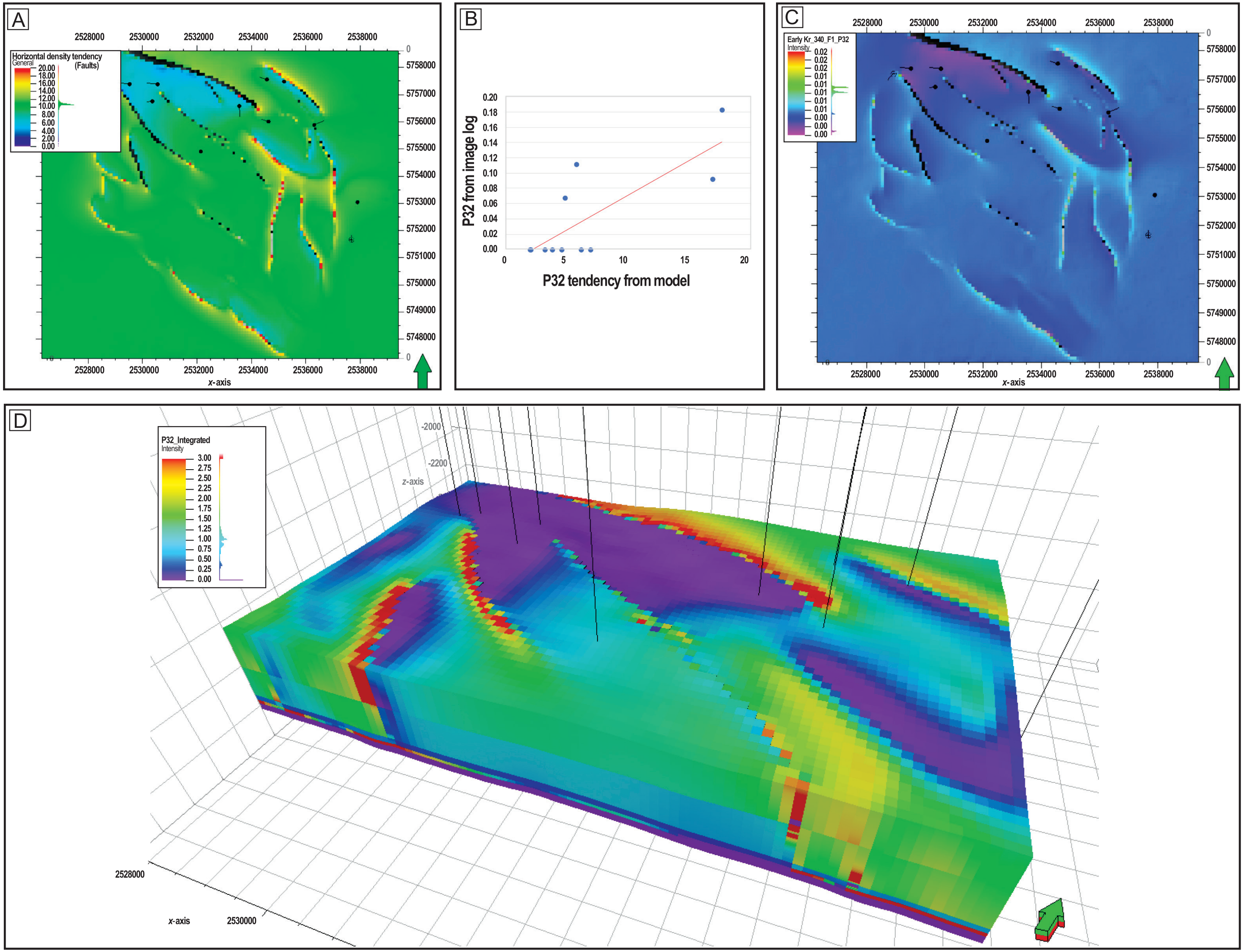

Figure 13. (A) Example of fracture tendency grid. Grids were constructed for each event (Lower Kr, Upper Kr, Tertiary, present-day) and fracture type (J, F_1, F_2). (B) Cross-plot of P32 as measured on the basis of image logs and P32 tendency calculated from model, as shown in (A). Near-zero values represent areas of low fracture intensity. All values were taken into account in the regression. (C) Example intensity grid constructed for Lower Cretaceous 340° F1 shear fractures by combining P32 from image logs and P32 tendency grid. Grids were constructed for each event and fracture type. (D) P32 fracture intensity distribution for all fracture types in the Loma Campana block.

Table 2. Parameters used in the construction of DFN models.

			Source	Value
Distribution	Vertical extension	Mesh zones, etc.	Mechanical stratigraphy	Variable
	Intensity	P10, P32	Mechanical model	0–5
Orientation	Dip, dip azimuth	Value and dispersion	Image logs	Variable by age
Geometry	Morphology	Number of sides	Outcrop	4
	Height, length	Value and dispersion	Outcrop	1 mm to 4 m long; 30 cm long (average)
		Height/length ratio	Outcrop	2:1 (average)
Dynamic properties	Aperture (hydraulic)	Value and dispersion	Outcrop/core	0.5 mm (average); 10% of kinematic
	Permeability	Value and dispersion	n/a	n/a

Fracture length, height, aspect ratio, and fracture morphology values were derived from a combination of outcrop and core observations and acoustic and resistivity borehole images. As information about fracture size from image logs and core was lacking, fracture dimensions measured in the Loncopué outcrops were used as a proxy to construct the DFN models. Fracture length ranges from 1 mm (0.04 in.) to 4 m (13 ft) were assumed, and a maximum fracture height of 2 m (7 ft) was used. All fractures were assumed to have a similar aspect ratio of 2:1, as estimated from outcrop observations. Fractures less than 1 m long were considered implicit and were treated as part of the host rock matrix; only fractures more than 1 m long made up the explicit network of fractures and were modeled. Fracture aperture (hydraulic) was calculated as the difference between kinematic aperture (perpendicular distance between two fracture walls irrespective of cement fill) and the percent fill observed in core samples, where porosity is typically between 5% and 10% or lesser. On the basis of core and outcrop observations, we assumed kinematic aperture to range between 0.1 mm and 2 cm (0.8 in.), with an average of 0.5 mm. The hydraulic aperture was assumed to be 10% of the kinematic aperture.

DFN Model Results

Figure 14 shows DFN models constructed for each modeled fracture set. The highest fracture intensity in the Loma Campana area is inferred to be for J and F_1 fractures formed under present-day state of stress and the lowest for present-day F_2 fractures. All other fracture sets show similar intensities, irrespective of their time of formation, and their distribution through the volume appears similar for each event, although their orientations are different (Figure 9). Note that this DFN was constructed specifically for the Loma Campana area and cannot be extrapolated to other areas of the Vaca Muerta play. Each area requires its own specific DFN.

DISCUSSION

Timing of Formation of Bed-Parallel and Bed-Perpendicular Fractures

Fluid inclusion microthermometry can be used to unlock the history of fracture growth (e.g., Fall et al., 2015). When correlated with burial- and thermal-history models, trapping temperatures of inclusions in synkinematic cements provide evidence of timing of fracture opening and cementation as long as the fluid and host rock were in thermal equilibrium. For the BPV and bed-perpendicular opening-mode fracture sets in the Arroyo Mulichinco outcrops, we contend that this was the case; the fluids were locally derived and were therefore in thermal equilibrium with the host rock. This might not be the case for faults. A comparison of trapping temperatures of inclusions in the different fracture sets in Arroyo Mulichinco outcrops (see “Outcrop Thermometry”, Figure 11) and a burial- and thermal-history curve for nearby Well A (Figure 1B) indicates BPV stages formed between 94 and 62 Ma, corresponding with the time of maximum burial in the Late Cretaceous (Figure 15A). Such fracture durations are comparable to fracturing rates estimated for tight-gas sandstones, which can last millions of

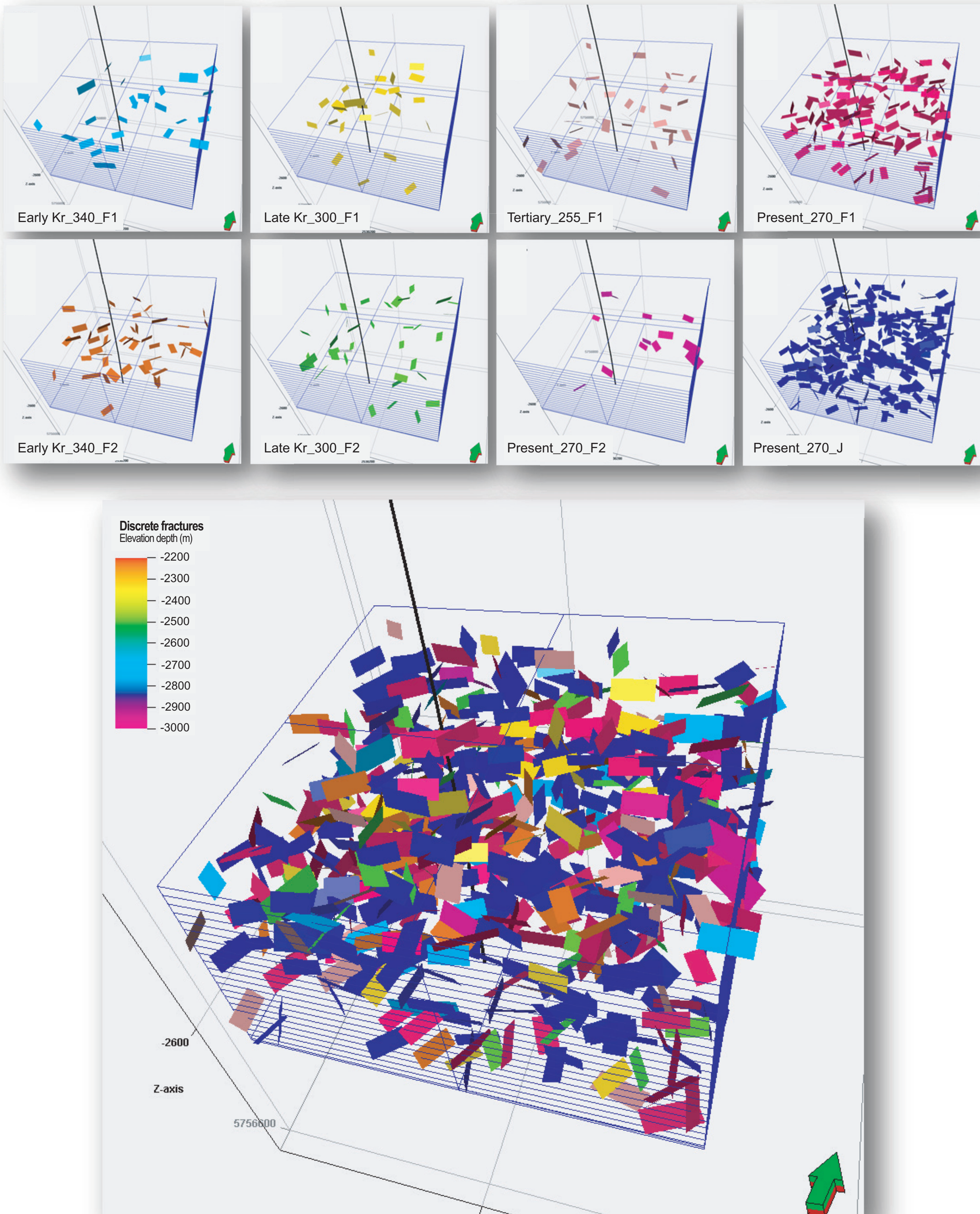

Figure 14. DFN models constructed for each event and each fracture type. Final DFN model (bottom) shows all fractures color-coded by age and type. DFN = discrete fracture network.

years (Becker et al., 2010; Fall et al., 2015, 2016), with many fractures forming near maximum burial conditions. These BPV ages are consistent with Maastrichtian to Miocene timing, which are inferred on the basis of ages of andesitic sills, laccoliths, and dykes that cross-cut BPV at Mulichinco (Sillitoe, 1977; Llambías and Rapela, 1989; Franchini et al., 2007; Rodrigues et al., 2009). The east–west, northwest–southeast, and north–south bed-perpendicular fracture sets formed in the Paleocene (~60–56 Ma). The timing of the northeast–southwest set could not be established owing to a lack of suitable fluid inclusions, although given cross-cutting relations, this set must have also formed in the Paleocene (Fall et al., 2017). Domal kinematic indicators are synchronous with the late-stage opening of BPV during bed-parallel east–west shortening in outcrop. Deformation in the Loncopué area was contractional in the east–west direction during the Late Cretaceous (Mosquera and Ramos, 2005; Rojas Vera et al., 2015), but the same orientation was present during the Paleogene from 30 to 26 Ma (Pardo-Casas and Molnar, 1987). Growth timing estimated for BPV using fluid inclusions (94–62 Ma) agrees with synchronous Late Cretaceous formation of domal structures near Loncopué.

On the basis of oxygen isotope analyses, Weger et al. (2019) concluded that BPV in the PC and YdT areas formed under higher temperature conditions than Vaca Muerta host rock. A comparison of clumped isotope data with published burial-history curves for PC suggests that BPV in this area formed between the Late Cretaceous and, potentially, through maximum burial conditions up to the Miocene (Figure 15B). In conjunction with Loncopué results, this finding suggests that BPV exposed in outcrop in the Andean foothills started to form in the Late Cretaceous, but BPV formation probably continued during subsequent burial, as also reported by Meissinger and Lo Forte (2014). Several episodes of BPV formation are supported by the observation that some BPV predate bed-perpendicular fractures, whereas others postdate them (as seen in SC cores). BPV formation was probably at its peak during maximum burial conditions. Weger et al. (2019), however, concluded that measured isotopic values for PC, YdT, SdlVM, and Loncopué BPV are slightly more depleted in $\delta^{18}O$ than those predicted by modeling of the extent of ^{18}O enrichment during recrystallization using the approach of Lawrence et al. (1975) and Killingley (1983) (Swart, 2000, 2015). This difference suggests that (1) deeper hydrothermal fluids with slightly higher temperatures were present during calcite cement precipitation, (2) that the presumed paleo-geothermal gradient in the Neuquén Basin was in fact higher than 35°C/km, and/or (3) the Vaca Muerta Formation was potentially buried more deeply than generally suggested (Weger et al., 2019, and references therein).

As suitable fluid inclusions for microthermometry in core or other data such as clumped isotopes are lacking, the absolute timing of formation of both bed-parallel and bed-perpendicular fractures in core cannot be inferred in this manner. Calcite within fractures (bed-perpendicular and BPV) in Core 1010 is more depleted in $\delta^{18}O$ than within the lower Vaca Muerta host rock, indicating that precipitation of calcite in fractures occurred under higher temperature conditions, after significant burial, than primary depositional calcite precipitation. These conditions are consistent with deep burial, which is inferred on the basis of bright-orange luminescence of these cements (Figure 8G; Hiatt and Pufhal, 2014). Therefore, as in outcrop, fractures in core postdate early diagenesis of Vaca Muerta mudrocks, in accordance with timing estimates in our tectonic model.

The presence of single- and two-phase, secondary, oil inclusions in bed-perpendicular fracture cements in core provides limited information about the timing of formation of these fractures. Secondary, oil inclusions indicate that the fractures were reactivated after primary cementation and after oil generation because oil must have been present in the system to become trapped as inclusions in the cements. In a recent study of bulk crushing analysis of fluid inclusions and nanopores in cuttings in a horizontal well in the Vaca Muerta Formation northwest of Loma Campana block, Hall et al. (2017) confirmed the secondary nature of oil inclusions relative to the fracture cements in core. These researchers found hydrocarbon species to C9, suggesting the presence of wet gas–to–gas condensate within the reservoir at the time of secondary fracturing.

Overpressure Conditions

Calcite fibers in BPV contain inclusions of hydrocarbons (Rodrigues et al., 2009; Cobbold et al., 2013; Zanella et al., 2015), and for aqueous inclusions, Rodrigues et al. (2009) measured homogenization temperatures in the range of 92°C to 113°C (198°F to 235°F) in the oil window with high overpressures (about halfway between hydrostatic and lithostatic). Given this evidence, formation of BPV in the Neuquén Basin has been related to overpressure during oil generation in the Cretaceous, when source rocks were maturing (Rodrigues et al., 2009; Cobbold et al., 2013). Near-lithostatic overpressure conditions during formation of BPV were confirmed by Fall et al. (unpublished results) for the Loncopué outcrops. If hydrocarbon generation commenced in the Neocomian, the time gap between early generation of hydrocarbons and BPV in the Late Cretaceous would be at

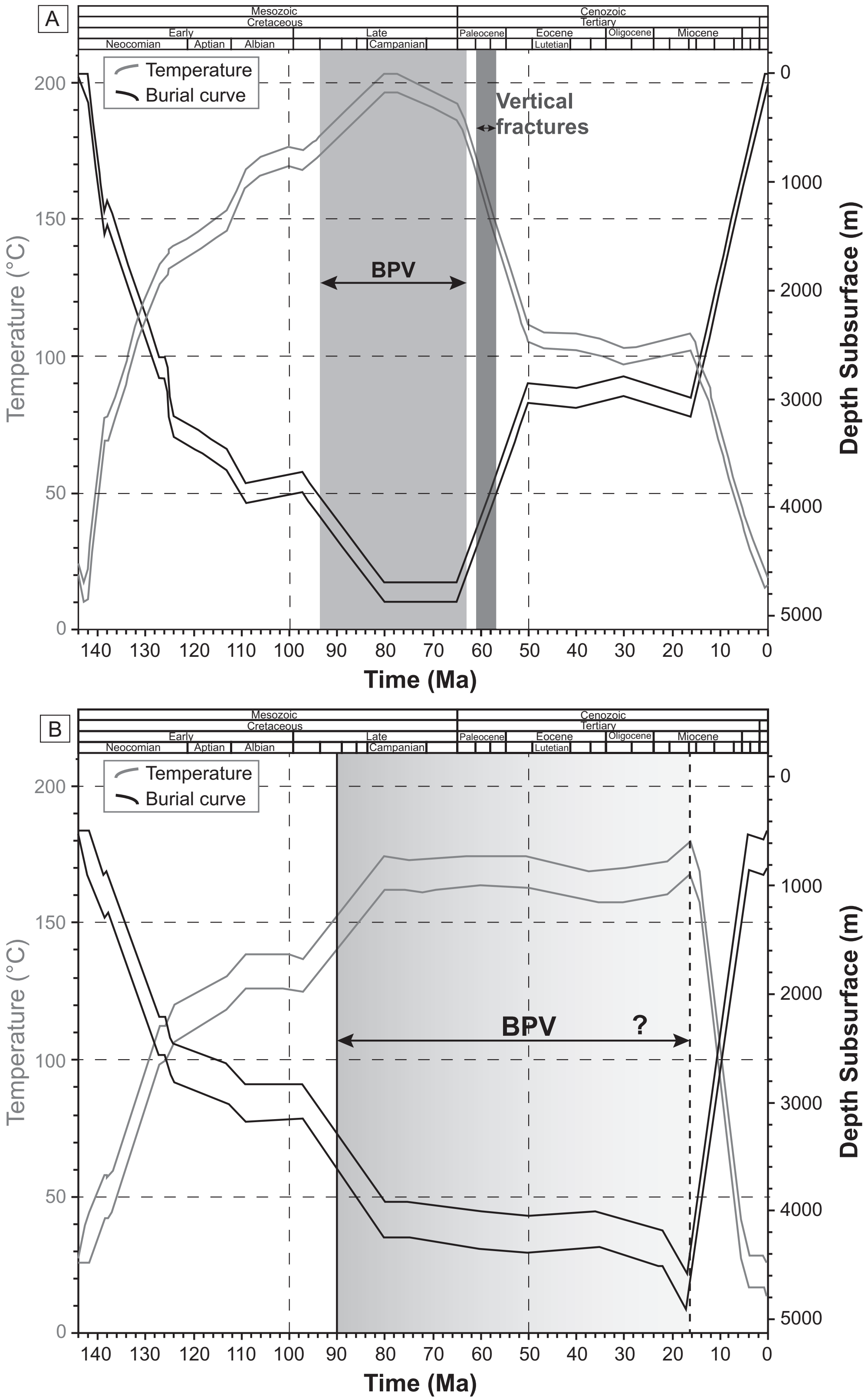

Figure 15. (A) Timing of formation of different fracture sets present at Arroyo Mulichinco estimated by correlating measured fluid inclusion temperatures with a burial-history curve constructed for nearby Well A. (B) Timing of formation of BPV at Puerta Curaco estimated by correlating calculated clumped isotope temperatures from Weger et al. (2019) with burial-history curve for a nearby well. BPV = bed-parallel veins.

least 30 m.y.—enough time for overpressures to build up in the reservoir. Overpressure conditions exist today in the buried Vaca Muerta Formation (Garcia et al., 2013; Fantín et al., 2014; Marchal et al., 2016).

Outcrop–to–Core Comparison

Orientations of fractures in the subsurface on the basis of image logs are similar to those measured in outcrop, except that the north–south set appears to be mostly absent in core, owing to a difference in the morphostructural context between the fold-and-thrust belt in outcrop and the embayment in core. Fractures in the east–west orientation appear to be dominant, at least in parts of the basin (Hernandez-Bilbao, 2016), as well as in outcrop, although fracture orientations can be influenced greatly by nearby fault systems (Gangui and Grausem, 2014; Santiago et al., 2014; Lazzari et al., 2015). On the basis of petrographic and SEM-CL evidence, Ukar et al. (2017c) concluded that the east–west set in outcrop was reactivated. This conclusion is consistent with fracture orientations being inferred in our tectonic model, suggesting that east–west fractures were actively opening during the Early Cretaceous and at present, too. North–south fractures in the Loncopué outcrops are parallel to the general fold–axis orientation in this area and may represent strike-parallel–fracture formation related to folding (e.g., Stearns, 1968), which is unique to the Vaca Muerta Formation section exposed in the fold-and-thrust belt. This would explain the absence of north–south fractures in core.

Similar fracture types were identified in outcrop and core across the basin, BPV being the most common type of fractures in both settings. The main difference between outcrop and core is fracture dimensions because BPV in outcrop is up to an order of magnitude wider than the widest fractures captured by core. Wide BPV in outcrop probably resulted from bed-perpendicular extension during early exhumation as well as bed-parallel contraction associated with folding as inferred from domal kinematic indicators (Ukar et al., 2017b). Domal structures that indicate bed-parallel contraction synchronous with BPV growth are also present in the subsurface and may be used either to infer paleo-stress orientation during formation of BPV or to orient core in cases where paleo-stress is independently known (Ukar et al., 2017b).

Both outcrop and core bed-perpendicular fractures show similar cements and amount of residual porosity, as well as a similar minimum aperture; fractures narrower than approximately 0.03 mm are absent in mudrock. Microfractures, however, are present cutting brittle beds such as marly layers and BPV. Measured apertures of the widest bed-perpendicular macrofractures are wider in outcrop possibly because of reactivation caused by folding (see Ukar et al., 2017b). Absence of similarly wide fractures in core may be because folding was less intense in the central part of the basin, or could reflect a sampling censoring bias, in which vertical cores do not capture them.

Fracture stratigraphy (e.g., Laubach et al., 2009) in the Vaca Muerta Formation consists of competent layers (BPV, altered tuffs, dolomitic marlstone) with mostly top-bound fractures. Widest macrofractures in competent layers persist into mudrock above and below, but microfractures are absent in mudrock—a hierarchical pattern. True fracture length and height dimensions are not measurable in core because of limited core dimensions, although fracture heights measured in both core and outcrop are in the range of a few centimeters to 1 m and appear similar.

Despite limited data for core, calculated bed-perpendicular fracture intensities and spacings are similar for outcrop and core (Figure 10). Fracture intensities for the narrowest fractures in core are similar to those measured in outcrop. Extrapolation of core data would result in a similar fracture abundance estimate of wide (>1 mm) macrofractures. Fracture abundance and spacing estimated using microscaling of bed-perpendicular fractures in altered tuff samples in core are therefore most likely good proxies for fracture intensity and spacing of fractures wider than 0.1 mm in mudrock, as shown by Ukar et al. (2017c) for outcrop. The lack of detected micro- and/or macrofractures that cut BPV in core is probably because of spacings being larger than the width of the core or difficulty in sample preparation and imaging of microfractures in such narrow BPV.

A proportional relationship between fracture spacing and layer thickness has been observed in many sedimentary rocks (Ladeira and Price, 1981; Narr and Suppe, 1991; Gross and Engeleder, 1995; Wu and Pollard, 1995; Bai and Pollard, 2000). In the Vaca Muerta Formation, the relationship is complex. Macrofractures in BPV are mostly regularly spaced (Figure 4C), and spacings tend to be narrower in thinner layers (although we did not quantify this relationship). However, in adjacent mudrock units that are several meters thick, macrofracture frequencies were found to be the same as for the BPV, so that the spacing–bed thickness relationship does not hold. Moreover, macrofractures in mudrock at Puesto are clustered around faults, and spacing is not related to bed thickness.

Comparison with Other Fractured Mudrocks

The suite of natural fractures observed in the Vaca Muerta Formation is comparable to those observed in other mudrocks (Gale et al., 2014). The biggest difference, perhaps, is in the degree to which BPV are developed. The thickest BPV, having the largest lateral extent in the world, occur in the now-exposed, deep, and most thermally mature section of the Neuquén Basin, in the Loncupué region. These are exceptional because of the high overpressure generated during hydrocarbon maturation and synchronous compression. The thermal input from volcanic activity in the region would have added to the maturation, and it has also been related to the formation of bitumen dykes during the Plio–Pleistocene (Cobbold et al., 2014). The BPV are less developed, although still present, in the less mature sectors of the Vaca Muerta play.

The relative timing of fractures of different types is also broadly consistent, although there are exceptions. In general, BPV seem to predate bed-perpendicular fractures. In the Marcellus, however, Wilkins et al. (2014) observed contemporaneous growth of kinematically compatible, vertical filled fractures, low-angle reverse faults, and stylolites in an overall contractional thrust–fault stress regime.

In general, the value of a comprehensive, natural fracture characterization would be in guiding decisions on play development or identification of sweet spots. As the interaction of hydraulic fractures and natural fractures is governed by multiple variables, however, there is no general solution, and site-specific information is needed to predict interaction behavior, which in turn, would inform decisions on whether to target or to avoid natural fractures. Well-constrained examples are needed to establish relationships between well production behavior and natural fracture systems; uncertainty of any such relationship is generally high because too many variables exist.

Tectonic and DFN Models: Lessons and Limitations

The Neuquén Basin has undergone a complex tectonic history, with several phases of extension and inversion, and DFN models must capture the relevant fracture network that is a culmination of the many phases of fracture growth. Inevitably, geomechanical modeling will be an oversimplification of these processes. The method outlined here does attempt to condition the models with data, however, allowing the locations of fracture clusters or corridors therefore to be assigned. Yet observations of clustering, regular spacing, or random distribution at different-length scales cannot be properly included. The key part of this study that differs from many superficially similar attempts is the inclusion of a timeline that spans the whole basin development, not just that of a single structure. The geomechanical conditions at the time of fracturing for many successive pulses of activity are incorporated, thus allowing for fractures of different origins and timing to be included in one model. Although advantageous in many ways, these models have important limitations. Independent constraints on deformation timing are desirable for reducing uncertainty in these models, but fracture timing modeled in this study for the Loma Campana area could not be corroborated owing to a lack of suitable fluid inclusion and/or clumped isotope temperatures tied to burial-history curves; this is a limitation of this case in particular and is not the result of a methodological constraint. Another main limitation is that because fracture propagation and concurrent cementation are not accounted for in the models, chemical–mechanical properties of older fractures do not change in successive steps. As fractures become partly cemented during growth, apertures, propagation, interaction, and permeability patterns change. For example, fractures tend to become preferentially cemented at their tips, arresting propagation and significantly altering effective permeability (Olson et al., 2009).

For calibrating present-day 3-D–stress geomechanical models DFN models were used, which constitute a main input for hydraulic fracture numerical simulators. Although the DFN models constructed in this study were directly comparable to well productivity, no direct relationship was found between production and the fracture geometry for each well. A direct relationship is lacking possibly because the factors controlling production go beyond the geometry of the hydraulic fracture (HF) network and are highly sensible to the completion approach, although the DFN models could be improved.

Permeability and Interaction with Hydraulic Fractures

Most fractures in outcrop and core are infilled by blocky and/or fibrous calcite cement. At least in some cases, bed-parallel and bed-perpendicular fractures are connected, as seen in some clear examples in core, and may have constituted a permeable network at the time of formation but are now mostly sealed. Present-day fluid flow through calcite-filled natural fractures is most likely to be limited. Fractures with apertures above the emergent threshold in populations that follow power-law distributions may preserve as much as between 25% and 40% residual unfilled pore space, although more commonly from 5% to 10% is preserved. Fluid flow through such partly open fractures may be significant in that their density is high enough, but for the most part, the P32 density of such fractures is extremely low. The P32 density is around 0.18 m^{-1} for all fractures measured in the Loma Campana image logs, which is below the low end of the range reported by Gale et al. (2014) for measured P32 densities in cores from other mudrocks (0.33–4.01 m^{-1}). The P32 for open fractures in this Vaca Muerta example would be a fraction of this measurement. Although natural fractures in the Vaca Muerta Formation may not provide fluid flow pathways in their natural state, they are probably not a barrier to flow. In a study of natural, calcite-filled fractures in the Eagle Ford Formation (South Texas, USA), Landry et al. (2016) found that permeability of fracture cement fill is comparable to that of the host rock.

Generally, elevated fluid pressures from hydraulic fracture treatments may cause reactivation of natural fractures, potentially opening them up to fluids and connecting them to the well bore via the HF network (Warpinski et al., 2005; Gale et al., 2007; Jeffrey et al., 2009). Narrow, sealed fractures may open or shear because the contact between the calcite fracture fill and the wall rock is weak (Gale et al., 2007). Wider, porous fractures, or those with inherent weakness in the cement, such as calcite cleavage planes or crack-seal planes, may break within the fracture thus capturing the propagating hydraulic fracture (e.g., Marcellus core in Lee et al., 2015). The hydraulic fracture network may grow in part by linking natural fractures, rather than by forming entirely new breaks (Gu et al., 2011; Chuprakov et al., 2014; Wu and Olson, 2016). Although such interaction may lead to a denser stimulation network that enhances production (Cipolla et al., 2008), not all stimulations result in improved production and flow rates.

Modeling of HF–natural fracture interactions in general has been done at different scales using different geomechanical approaches. Some studies focus on interaction at the small scale close to the intersection (e.g., Dahi-Taleghani and Olson, 2011, 2014; Zhang et al., 2017), whereas others focus on larger scale stress perturbations (e.g., Shrivastava and Sharma, 2018). In published studies of modeling in the Vaca Muerta Formation, there are several different approaches. Haddad et al. (2017) tried 3-D HF modeling with integrated microseismic data. Their modeling results demonstrate natural fracture reactivation and HF growth complexities at the intersections, such as height throttling, sharp aperture size reduction, and fracture branching. Alderete et al. (2017) modeled the HF network in nonfractured rock using a coupled fluid–structure interaction model in a poro-elastic medium. The model considers rock anisotropy that is based on data from sonic logs in Vaca Muerta wells. The authors preconditioned the HF path and found that natural fractures can be added to the model, although they did not show such an example.

Sagasti et al. (2014) noted the importance of multiscale sedimentological, petrophysical, and geomechanical heterogeneity on hydraulic fracture growth. In their study of the Vaca Muerta Formation at field and well scale, they integrated core, log, and seismic data to document these heterogeneities. They found that the uppermost part of the Vaca Muerta Formation has the lowest heterogeneity and frequency of weak interfaces and, therefore, the potential for developing hydraulic fractures with greater height growth and conductivity than in the other intervals. Sagasti et al. (2014) also considered the relative position between perforations in the well and the heterogeneities they describe. If a horizontal well is located in a highly heterogeneous interval, there is a risk of disconnecting a large part of the hydraulic fracture from the wellbore. They noted that the effect is greater in a horizontal well, where perforations are all in the same stratigraphic unit; the risk is reduced in vertical wells because the perforations are in multiple stratigraphic units. Although they focused on other heterogeneities, a similar argument could apply to the effect of natural fractures.

Monti et al. (2013) discussed the potential for developing the Vaca Muerta Formation using vertical wells because of its thickness, focusing on Loma La Lata and Loma Campana development areas. They approached the problem using production decline analysis, which is an indirect way of gaining information about HF geometry and has been applied to other mudrock production studies (e.g., Patzek et al., 2014). Monti et al. (2013) included numerical modeling of multiple HFs in a multilayer, looking at the stimulated rock volume (SRV) and undisturbed matrix beyond the SRV. They observed linear flow followed by boundary-dominated flow, noting that linear flow may be caused by the presence and reactivation of natural fractures. This approach is fundamentally different from modeling of HF growth, but it could be used to test DFN models. Nowadays, however, vertical wells in the Vaca Muerta Formation are used for extraction of core but are not targeted for production because of the economic superiority of horizontal wells.

In this chapter, we have shown that HFs in the Vaca Muerta Formation are most likely to encounter natural fractures, which are observed in most cores. Vertical HF growth would be impacted by BPV, whereas bed-perpendicular natural fractures would impact lateral HF growth. Lee et al. (2015) showed that angle of approach and thickness of a natural fracture control whether an HF will arrest at a natural fracture, divert and propagate along or within it, or propagate straight across. The behavior will be governed by the energy release involved in each of these possibilities and will also depend on the energy behind the HF. The interaction of an HF with a given natural fracture might therefore be different, depending on whether the encounter is near the wellbore or distant from it. Added to this complexity is the fact that natural fractures follow aperture size population distributions (power law or negative exponential), in which there are many narrow fractures and relatively fewer thick ones.

Present-day maximum horizontal stress trends approximately east–west in the Neuquén Basin (80°–100°) (Guzmán and Cristallini, 2009; Varela et al., 2020, this Memoir), and because this direction is nearly parallel to dominant natural fractures, reactivation of preexisting natural fractures is potentially high. Microseismic imaging shows that hydraulic fractures in the area of Loma Campana propagate in three main orientations (Lazzari et al., 2015): conspicuous propagation occurring at N280° to N290°, which coincides with the orientation of present-day maximum horizontal stress and the orientation of the highest fracture intensity (J) modeled for this area (Figures 12, 14), the other two orientations being N240° and N210°. The N240° orientation coincides with F2 fractures forming under current state-of-stress configuration, whereas fractures in the N210° orientation probably indicate reactivation of Upper Cretaceous natural fractures, as modeled in this study, during hydraulic stimulation.

Microfractures in the Vaca Muerta Formation are clustered at small-length scales, but because these fractures are narrow, they are less likely to divert an HF—even clusters may have little effect. The wider, more regularly spaced fractures are more likely to divert a hydraulic fracture, as in the Haddad et al. (2017) study. Maxwell et al. (2015) recognized that microseismicity induced by hydraulic fracturing can include both wet microseismic events directly associated with hydraulic fracturing and remote dry events. Weak fractures of any size may open or shear owing to perturbation of the stress field away from any HF. At the time of writing, we did not know of microseismic data indicating bed-parallel propagation of HFs in the Vaca Muerta. Because other studies have observed and modeled this phenomenon (Rutledge et al., 2014; Tan and Engelder, 2016), however, such data could be expected, given the relatively high intensity and thickness of BPV in the Vaca Muerta Formation relative to other mudrocks.

In practice, many HF simulators cannot directly incorporate DFN model outputs, and oversimplifications are necessary. For example, in some simulators, all natural fractures are considered vertical, but cores and outcrop show that dip variations in the Vaca Muerta Formation are large. Likewise, such models cannot account for layer-parallel fractures, which are among the most abundant types of fractures in the Vaca Muerta Formation. Therefore, study of the impact of natural fractures on HF geometry and efficiency is challenging, owing to oversimplifications, although substantial efforts are underway to improve these approximations.

CONCLUSIONS

In this chapter, we have shown that abundant natural fractures exist in the Vaca Muerta Formation, both in outcrops and in the subsurface. Bed-parallel veins (BPV), bed-perpendicular fractures, early ptygmatic fractures, low-angle fractures, and faults are present, these natural fractures are similar to those observed in other mudrocks. The most abundant and one of the oldest types of fracture are BPV, and in core and outcrop populations, they follow a negative exponential aperture size distribution. A weak relationship exists between BPV abundance and TOC content of the host rock, and BPV commonly develop along mechanical layer interfaces. As many as four sets of bed-perpendicular fractures occur in mudrock and in competent layers including BPV, altered tuffs, and dolomitic marlstones. Clustered microfractures form part of the populations in competent layers, but microfractures are absent in mudrock and BPV in the subsurface. Bed-perpendicular fracture populations follow power-law aperture size distributions. In outcrops near the Cerro Mocho area, east of Loncopué, two main bed-perpendicular opening mode fracture sets are oriented east–west (oldest) and north–south (youngest), and two additional sets (northeast–southwest and northwest–southeast) are locally present. Heights of bed-perpendicular fractures rarely extend beyond 2 m (7 ft); height pattern is overall hierarchical but tends toward top-bounded within some of the competent layers (c.f. Hooker et al., 2013). Spacings of bed-perpendicular fractures (≥0.1 mm in aperture) range from approximately 0.3 mm to about 2 m (7 ft) with the highest fracture abundance being near faults. Fracture cements are dominated by calcite, but minor amounts of quartz, pyrite, gypsum, siderite, and/or bitumen are present in some fractures. Both bed-parallel and bed-perpendicular fractures may have acted as fluid pathways contributing to oil migration.

The orientations, dimensions, cements, intensities, and spacings of natural fractures are similar in Vaca Muerta Formation outcrops and cores, although with important differences, the biggest difference being the higher abundance and larger size of BPV in outcrops. As much as 10% of the volume of the rock in outcrop may be of BPV, and 10-cm-thick BPV are common. In core, the widest BPV are about 2 cm, and spacings are on the order of 0.5 to 1 m (3 ft), although BPV are more abundant at the TOC-rich base of the formation. A second difference is that in outcrop, most bed-perpendicular fractures are oriented east–west and north–south, whereas in the subsurface east–west fractures are predominant. We propose that such differences are reflective of differences in the tectonic and diagenetic history of rocks exposed in the Agrio fold-and-thrust belt as compared with those currently in the embayment of the Neuquén Basin.

A comparison of fluid inclusion and clumped isotope temperatures with burial-history curves allow establishment of the absolute timing of formation of BPV and bed-perpendicular fractures in outcrop. In the Loncopué area, BPV formed near maximum burial conditions in the Late Cretaceous, whereas bed-perpendicular fractures formed in the Paleocene. In Puerta Curaco, BPV formation started in the Late Cretaceous but most likely continued during subsequent burial until the Miocene. Nucleation of BPV was probably at its peak during maximum burial, aided by strong overpressure conditions. Those BPV now exposed in outcrop continued to widen during exhumation owing to decompression, fold-related shear, and bed-parallel contraction during BPV formation in the fold-and-thrust belt. Fracture cement geochemistry indicates the outcrops near Loncopué are of similar maturity to the most mature parts of the Vaca Muerta reservoir and can be used as guides for this part of the basin.

In core, BPV lack fluid inclusions suitable for microthermometry but based on cross-cutting relationships BPV are some of the oldest types of fracture in the subsurface, and stable isotope analyses indicate they formed deep in the subsurface probably under conditions similar to those inferred for outcrops. Tectonic modeling suggests that bed-perpendicular fractures in the subsurface of the Loma Campana block formed during Early Cretaceous, Late Cretaceous, Tertiary, and continuing at present. Tectonic models indicate that the most abundant types of fractures are opening-mode fractures forming under the current state of stress. Most fractures are infilled by blocky and/or fibrous calcite cement and P32 fracture densities in Loma Campana are low (0.18 m^{-1}), except adjacent to faults. Therefore, present-day fluid flow through natural fractures is likely to be limited to the few open fractures above the emergent threshold (~0.1 mm for core), and to nanoscale flow along crystal boundaries in the cement (c.f. Landry et al., 2016). However, reactivation of preexisting natural fractures by hydraulic fractures is potentially high because present-day maximum horizontal stress trends approximately east–west in the Neuquén Basin, coinciding with the direction of dominant natural fractures. Reactivation of bed-perpendicular fractures has been supported by microseismic data. Given the relatively high intensity of BPV in the Vaca Muerta Formation relative to other mudrocks, reactivation of BPV during hydraulic treatments is also expected.

ACKNOWLEDGMENTS

We would like to thank our many field assistants (Diego Licitra, Sebastían Paulin, Julián Fantín, Rosina Barberis, Carolina González, Victoria Lazzari, Matías Cáneva, Juan Pablo Álvarez, Martín Foster, and Juan Pablo Catalano) and Iván Lanusse Noguera for laying the groundwork for an outcrop and core comparative study in the Vaca Muerta Formation. The study of fractures in the 1010 Core was supported by The Vaca Muerta Consortium of the Colorado School of Mines. We thank Dr. David A. Budd for help with optical-CL imaging, Sara Elliott for assistance with SEM-CL image mosaicking, Qiqi Wang for core sample scans, Jessica Franklin for seismic images, and Larry Meckel for providing many helpful discussions and great enthusiasm. Thanks to Pampa Energía SA and its partners in the Sierra Chata and Parva Negra Este blocks. This manuscript benefited greatly from careful revisions by Bill Derschowitz, Orlando Ortega, and Nuno Rodrigues. Publication has been authorized by the Director, Bureau of Economic Geology.

REFERENCES CITED

Al Dulhailan, M. A., and S. A. Sonnenberg, 2015, Analyzing beef fractures: Genesis and relationship with organic-rich shale facies: Unconventional Resources Technology Conference, DOI: 10.15530/URTEC-2015-2151959.

Alderete, I. D., A. Sosa-Massaro, and S. D'Hers, 2017, A fluid structure interaction model for hydraulic fracture simulation on Vaca Muerta Argentina shale formation: SPE Latin America and Caribbean Petroleum Engineering Conference, Buenos Aires, Argentina, 17–19 May, DOI: 10.2118/185563-MS.

Anderson, E. M., 1905, The dynamics of faulting, reprinted *in* D. Healy, R. W. H. Butler, Z. K. Shipton, and R. H. Sibson, eds., 2012, Faulting, fracturing and igneous intrusion in the Earth's crust: London, The Geological Society, Special Publication 367, p. 231–246.

Armella, C., N. Cabaleri, and H. A. Leanza, 2007, Tidally dominated, rimmed-shelf facies of the Picún Leufú Formation (Jurassic/Cretaceous boundary) in southwest

Gondwana, Neuquén Basin, Argentina: Cretaceous Research, v. 28, no. 6, p. 961–979.

Arregui, C., 1993, Análisis estratigráfico-paleoambiental de la Formación Tordillo en el subsuelo de la Cuenca Neuquina: 12° Congreso Geológico Argentino, Mendoza, Argentina 10–15 October, Actas 1, p. 165–169.

Bai, T., and D. D. Pollard, 2000, Closely spaced fractures in layered rocks: Initiation mechanism and propagation kinematics: Journal of Structural Geology, v. 22, p. 1409–1425.

Becker, S. P., P. Eichhubl, S. E. Laubach, R. M. Reed, R. H. Lander, and R. J. Bodnar, 2010, A 48-m.y. history of fracture opening, temperature, and fluid pressure: Cretaceous Travis Peak Formation, East Texas Basin: Geological Society of America Bulletin, v. 122, p. 1081–1093, DOI: 10.1130/B30067.1.

Brooks, B., M. Bevis, R. Smalley Jr., E. Kendrick, R. Manceda, E. Lauría, R. Maturana, and M. Araujo, 2003, Crustal motion in the Southern Andes (26°–36°S): Do the Andes behave like a microplate?: Geochemistry Geophysics Geosystems, v. 4, no. 10, p. 1–14.

Buckland, W., and H. T. De la Beche, 1835, On the geology of the neighbourhood of Weymouth and the adjacent parts of the coast of Dorset: Transactions of the Geological Society, London, s2–4, p. 1–46.

Chuprakov, D., A. Melcheava, and R. Prioul, 2014, Injection-sensitive mechanics of hydraulic fracture interaction with discontinuities: Rock Mechanics and Rock Engineering, v. 47, no. 5, p. 1625–1640, DOI: 10.1007/s00603-014-0596-

Cipolla, C. L., N. R. Warpinski, M. J. Mayerhofer, and E. P. Lolon, 2008, The relationship between fracture complexity, reservoir properties, and fracture-treatment design: SPE Annual Technical Conference and Exhibition, Denver, Colorado, USA, 21–24 September, p. 438–452, DOI: 10.2118/115769-MS.

Cobbold, P., and E. Rossello, 2003, Aptian to recent compressional deformation, foothills of the Neuquén Basin, Argentina: Marine and Petroleum Geology, v. 20, p. 429–443.

Cobbold, P. R., A. Zanella, N. Rodrigues, and H. Løseth, 2013, Bedding-parallel fibrous veins (beef and cone-in-cone): Worldwide occurrence and possible significance in terms of fluid overpressure, hydrocarbon generation and mineralization: Marine and Petroleum Geology, v. 43, p. 1–20.

Cobbold, P. R., G. Ruffet, L. Leith, H. Loseth, N. Rodrigues, H. A. Leanza, and A. Zanella, 2014, Radial patterns of bitumen dykes around quaternary volcanoes, provinces of northern Neuquén and southernmost Mendoza, Argentina: Journal of South American Earth Sciences, v. 56, p. 454–467.

Cole, G. A. J., 1893, On some examples of cone-in-cone structure: Mineralogical Magazine, v. 10, p. 136–141.

Cristallini, E., R. Tomezzoli, G. Pando, C. Gazzera, J. M. Martínez, J. Quiroga, M. Buhler, F. Bechis, S. Barredo, and O. Zambrano, 2009, Controles precuyanos en la estructura de la Cuenca Neuquina: Revista de la Asociación Geológica Argentina, v. 65, no. 2, p. 248–264.

Cruz, C. E., H. J. Villar, and G. Nelson Munoz, 1996, Los sistemas petroleros del Grupo Mendoza en la Fosa de Chos Malal: Cuenca Neuquina, Argentina: 13° Congreso Geologico Argentino, Buenos Aires, Argentina, 13–18 October, Actas 1, p. 45–60.

Dahi-Taleghani, A., and J. E. Olson, 2011, Numerical modeling of multistranded-hydraulic-fracture propagation: Accounting for the interaction between induced and natural fractures: SPE Journal, v. 16, no. 3, p. 575–581.

Dahi-Taleghani, A., and J. Olson, 2014, How natural fractures could affect hydraulic fracture geometry: SPE Journal, v. 19, no. 1, p. 161–171.

De Barrio, A., P. Ferraresi, G. Köhler, D. Marchal, and S. Blanco, 2018, Estudio comparativo de testigos corona de las dos secciones enriquecidas de la Formación Vaca Muerta en la zona de shale gas, noroeste del Engolfamiento Neuquino: Revista de la Asociación Geológica Argentina, v. 75, no. 2, p. 243–252.

Dershowitz, W. S., and H. H. Herda, 1992, Interpretation of fracture spacing and intensity: American Rock Mechanics Association, 33rd U.S. Symposium on Rock Mechanics (USRMS), Santa Fe, New Mexico, USA, 3–5 June, accessed April 10, 2019, https://www.onepetro.org/conference-paper/ARMA-92-0757.

Domínguez, R. F., I. Lanusse Noguera, M. J. Continanzia, K. Mykietiuk, C. Ponce, G. Pérez, R. Guerello, et al., 2016, Organic-rich stratigraphic units in the Vaca Muerta Formation and their distribution and characterization in the Neuquén Basin (Argentina): Unconventional Resources Technology Conference, San Antonio, Texas, USA, 1–3 August, p. 1439–1450, accessed April 10, 2019, DOI: 10.15530/URTEC-2016-2456851.

Du, C. M., X. Zhang, Y. Z. Ma, P. Kaufman, B. Melton, and S. Gowelly, 2011, Integrated shale gas reservoir modeling, *in* Y. Z. Ma, and P. R. La Pointe, eds., Uncertainty analysis and reservoir modeling: AAPG Memoir 96, p. 265–280.

Fall, A., P. Eichhubl, R. J. Bodnar, S. E. Laubach, and J. S. Davis, 2015, Natural hydraulic fracturing of tight-gas sandstone reservoirs, Piceance Basin, Colorado: Geological Society of America Bulletin, v. 127, p. 61–75, DOI: 10.1130/B31021.1.

Fall, A., E. Ukar, and S. E. Laubach, 2016, Origin and timing of Dauphiné twins in quartz cement in fractured sandstones from diagenetic environments: Insight from fluid inclusions: Tectonophysics, v. 687, p. 195–209.

Fall, A., E. Ukar, R. G. Lopez, J. F. W. Gale, R. Manceda, and S. E. Laubach, 2017, Combined effects of overpressure and bed-parallel contraction on the formation of bed-parallel and vertical fractures in the Vaca Muerta Formation, Argentina: Geological Society of America Annual Meeting, Seattle, Washington, USA, 22–25 October, v. 49, no. 6, DOI: 10.1130/abs/2017AM-301560.

Fall, A., and R. J. Bodnar, 2018, How precisely can the temperature of a fluid event be constrained using fluid inclusions?: Economic Geology, v. 113, p. 1817–1843.

Fantín, M., L. Crousse, S. Cuervo, D. Vallejo, F. González Tomassini, H. Reijenstein, and C. Lipinski, 2014, Vaca Muerta stratigraphy in central Neuquén Basin: Impact on emergent unconventional project: Unconventional Resources Technology Conference, Denver, Colorado, USA, 25–27 August, DOI: 10.15530/URTEC-2014-1923793.

Franchini, M., A. Impiccini, L. Meinert, G. Grathoff, and I. B. A. Schalamuk, 2007, Clay mineralogy and zonation in the Campana Mahuida Porphyry Cu deposit, Neuquén, Argentina: Implications for porphyry Cu exploration: Economic Geology, v. 102, p. 27–54.

Franklin, J., 2016, Integrated three-dimensional geological model of the Vaca Muerta Formation in the Loma Jarillosa Este area, Neuquén Basin, Argentina, Master's thesis, Colorado School of Mines, 134 p.

Franks, P. C., 1969, Nature, origin, and significance of cone-in-cone structures in the Kiowa Formation (Early Cretaceous), north-central Kansas: Journal of Sedimentary Petrology, v. 39, p. 1438–1454.

Gale, J. F. W., R. M. Reed, and J. Holder, 2007, Natural fractures in the Barnett Shale and their importance for hydraulic fracture treatments: AAPG Bulletin, v. 91, no. 4, p. 603–622, DOI: 10.1306/11010606061.

Gale, J. F. W., S. E. Laubach, J. E. Olson, P. Eichhubl, and A. Fall, 2014, Natural fractures in shale: A review and new observations: AAPG Bulletin, v. 98, no. 11, p. 2165–2216.

Gangui, A., and M. Grausem, 2014, Tectonismo y estilos estructurales en el Engolfamiento Neuquino: Implicancias en la interpretación de las fracturas monitoreadas por microsísmica en la formación Vaca Muerta, *in* S. Galeazzi, G. González, M. Santiago, D. García, L. Maschio, R. González, and J. Ramírez Martínez, eds., 9° Congreso de Exploración y Desarrollo de Hidrocarburos, Simposio de Recursos No Convencionales, Mendoza, Argentina, 3–7 November, p. 341–364.

Garcia, M. N., F. Sorenson, J. C. Bonapace, F. Motta, C. Bajuk, and H. Stockman, 2013, Vaca Muerta shale reservoir characterization and description: The starting point for development of a shale play with very good possibilities for a successful project: Unconventional Resources Technology Conference, Denver, Colorado, USA, 12–14 August, accessed April 10, 2019, DOI: 10.15530/URTEC-1508336-MS.

Ghosh, P., J. Adkins, H. Affek, B. Balta, W. Guo, E. A. Schauble, D. P. Schrag, and J. M. Eiler, 2006, ^{13}C–^{18}O bonds in carbonate minerals: A new kind of paleothermometer: Geochimica et Cosmochimica Acta, v. 70, p. 1439–1456.

Goldstein, R. H., and T. J. Reynolds, 1994, Systematics of fluid inclusions in diagenetic minerals: SEPM (Society for Sedimentary Geology) Short Course 31, 199 p.

Gross, M. R., and T. Engeleder, 1995, Strain accommodated by brittle failure in adjacent units of the Monterey Formation, U.S.A.: Scale effects and evidence for uniform displacement boundary conditions: Journal of Structural Geology, v. 17, p. 1303–1318.

Gu, H., X. Weng, J. Lund, M. Mack, U. Ganguly, and R. Suarez-Rivera, 2011, Hydraulic fracture crossing natural fracture at non-orthogonal angles: A criterion, its validation and applications: SPE Hydraulic Fracturing Conference and Exhibition, The Woodlands, Texas, USA, 24–26 January, 11 p., accessed April 10, 2019, DOI: 10.2118/139984-PA.

Gutiérrez-Schmidt, N., J. C. Alonso, A. Giusiano, C. Lauri, and T. Sales, 2014, El shale de la formación Vaca Muerta: Integración de datos y estimación de recursos de petróleo y gas asociado, provincia de Neuquén: 9° Congreso de Exploración y Desarrollo de Hidrocarburos, Simposio de Recursos no Convencionales: Ampliando el Horizonte Energético, Mendoza, Argentina, 3–7 November, p. 795–813.

Guzmán, C., 2007, Estudio de la deformación andina entre los 32° y los 39° latitud sur mediante el análisis de breakout de pozos, Universidad de Buenos Aires, Tésis doctoral, 241 p.

Guzmán, C. G., and E. O. Cristallini, 2009, Contemporary stress orientations from borehole breakout analysis in the southernmost flat-slab boundary Andean retroarc (32°44'and 33°40'S): Journal of Geophysical Research, v. 114, p. B02406, DOI: 10.1029/2007JB005505.

Haddad, M., J. Du, and S. Vidal-Gilbert, 2017, Integration of dynamic microseismic data with a true 3D modeling of hydraulic-fracture propagation in the Vaca Muerta shale: SPE Journal, Volume 22, Issue 6, p. 1714–1838. SPE-179164-PA. https://doi.org/10.2118/179164-PA., DOI: 10.2118/179164-PA.

Hall, D. L., M. Fasola, and D. Strapoc, 2017, Advanced mud gas and fluid inclusion analysis–Vaca Muerta Horizontal, Argentina: AAPG Search and Discovery Article 90291, accessed April 10, 2019, http://www.searchanddiscovery.com/abstracts/html/2017/90291ace/abstracts/2603721.html.

Hernandez-Bilbao, E., 2016, High-resolution chemostratigraphy, sequence stratigraphic correlation, porosity and fracture characterization of the Vaca Muerta Formation, Neuquén Basin, Argentina, Ph.D. dissertation, Colorado School of Mines, 195 p.

Hiatt, E. E., and P. K. Pufahl, 2014, Cathodoluminescence petrography of carbonate rocks: A review of applications for understanding diagenesis, reservoir quality, and pore system evolution, *in* I. Coulson, ed., Cathodoluminescence and its application to geoscience: Mineralogical Association of Canada, Fredericton, New Brunswick, Short Course Series Volume 45, p. 75–96.

Hooker, J. N., and J. Cartwright, 2016, Dolomite overgrowths suggest a primary origin of cone-in-cone: Geological Magazine, v. 155, p. 568–585, DOI: 10.1017/S0016756816000807.

Hooker, J. N., J. W. Gale, L. A. Gomez, S. E. Laubach, R. R. Marrett, and R. M. Reed, 2009, Aperture-size scaling variations in a low-strain opening-mode fracture set, Cozzette Sandstone, Colorado: Journal of Structural Geology, v. 31, p. 707–718, DOI: 10.1016/j.jsg.2009.04.001.

Hooker, J. N., S. E. Laubach, and R. Marrett, 2013, Fracture-aperture size–frequency, spatial distribution, and growth processes in strata-bounded and non-strata-bounded fractures, Cambrian Mesón Group, NW Argentina: Journal of Structural Geology, v. 54, p. 54–71, DOI: 10.1016/j.jsg.2013.06.011.

Hryb, D., and R. G. Lopez, 2015. MoTeL software, Modelado Tectonico Libre: YPF, Internal Development.

Hryb, D., R. G. Lopez, and R. Manceda, 2018, Tectonic history validation in a multiphase deformation basin using natural fracture system, Vaca Muerta Formation, Argentina: 2nd International Discrete Fracture Network Engineering Conference, Seattle, Washington, USA, 20–22 June, ARMA-DFNE-18-0855, accessed April 10, 2019, https://www.onepetro.org/conference-paper/ARMA-DFNE-18-0855.

Jaillard, E., P. Soler, G. Carher, and T. Mourier, 1990, Geodynamic evolution of the northern and central Andes during early to middle Mesozoic times: A Tethyan model: Journal of the Geological Society, London, v. 147, p. 1009–1022.

Jeffrey, R. G., X. Zhang, and M. Thiercelin, 2009, Hydraulic fracture offsetting in naturally fractured reservoirs: Quantifying a long-recognized process: SPE Hydraulic Fracturing Technology Conference, The Woodlands, Texas, USA, 19–21 January, 15 p., DOI: 10.2118/119351-MS.

Kietzmann, D. A., F. González Tomassini, and T. Smith, 2020, Grain association, petrography, and lithofacies, *in* D. Minisini, M. Fantín, I. Lanusse Noguera, and H. A. Leanza, eds., Integrated geology of unconventionals: The case of the Vaca Muerta play, Argentina: AAPG Memoir 121, p. XX–XX.

Killingley, J. S., 1983, Effects of diagenetic recrystallization on $^{18}O/^{16}O$ values of deep-sea sediments: Nature, v. 301, p. 594–597.

Kozlowski, S., C. E. Cruz, and C. Sylwan, 1998, Modelo exploratorio en la faja corrida de la Cuenca Neuquina, Argentina: Boletín de Informaciones Petroleras, v. 55, p. 4–23.

Ladeira, F. L., and N. J. Price, 1981, Relationship between fracture spacing and bed thickness: Journal of Structural Geology, v. 3, no. 2, p. 179–183.

Larmier, S., A. Zanella, A. Lejay, R. Mourgues, and F. Gelin, 2018, Distribution of natural hydraulic fractures (beef veins) within the Vaca Muerta Formation, Neuquén Basin, Argentina: AAPG ACE Annual Convention and Exhibition, Salt Lake City, Utah, USA, 23–25 July, accessed April 10, 2019, http://www.searchanddiscovery.com/abstracts/html/2018/ace2018/abstracts/2855581.html.

Lander, R. H., and S. E. Laubach, 2015, Insights into rates of fracture growth and sealing from a model of quartz cementation in fractured sandstones: Geological Society of America Bulletin, v. 127, p. 516–538, DOI: 10.1130/B31092.1.

Landry, C. J., P. Eichhubl, M. Prodanović, and S. Wilkins, 2016, Nanoscale grain boundary channels in fracture cement enhance flow in mudrocks: Journal of Geophysical Research: Solid Earth, v. 121, no. 5, p. 3366–3376, DOI: 10.1002/2016JB012810.

Laubach, S. E., 2003, Practical approaches to identifying sealed and open fractures: AAPG Bulletin, v. 87, p. 561–579.

Laubach, S. E., J. E. Olson, and M. R. Gross, 2009, Mechanical and fracture stratigraphy: AAPG Bulletin, v. 93, p. 1413–1426.

Lawrence, J., J. Gieskes, and W. Broecker, 1975, Oxygen isotope and cation composition of DSDP pore waters and the alteration of Layer II basalts: Earth and Planetary Science Letters, v. 27, p. 1–10.

Lazzari, V., D. Hryb, R. Manceda, and M. Foster, 2015, Predicción de fracturas naturales en la formación Vaca Muerta: Petrotecnia, p. 64–77.

Leanza, H. A., 1973, Estudio sobre los cambios faciales de los estratos limítrofes jurásico-cretácicos entre Loncopué y Picún-Leufú, Provincia de Neuquén, República Argentina: Revista de la Asociación Geológica Argentina, v. 28, p. 97–132.

Leanza, H. A., 2003, Las sedimentitas huitrinianas y rayosianas (Cretácico inferior) en el ámbito central y meridional de la Cuenca Neuquina, Argentina, SEGEMAR, Serie Contribuciones Técnicas: Geología, v. 2, p. 1–31.

Leanza, H. A., 2009, Las principales discordancias del Mesozoico de la Cuenca Neuquina según observaciones de superficie: Revista del Museo Argentino de Ciencias Naturales, Nueva Serie, v. 11, no. 2, p. 145–184.

Leanza, H. A., F. Sattler, R. S. Martinez, and O. Carbone, 2011, La Formación Vaca Muerta y equivalentes (Jurásico Tardío–Cretácico Temprano) en la Cuenca Neuquina, *in* Geología y Recursos Naturales de la Provincia del Neuquén, Neuquén, p. 113–129.

Lee, H. P., J. E. Olson, J. Holder, J. F. W. Gale, and R. D. Myers, 2015, The interaction of propagating opening mode fractures with preexisting discontinuities in shale: Journal of Geophysical Research: Solid Earth, v. 120, p. 169–181.

Legarreta, L., and C. Gulisano, 1989, Análisis estratigráfico secuencial de la Cuenca Neuquina (Triásico superior–Terciario inferior), Cuencas sedimentarias argentinas: Universidad Nacional de Tucumán, San Miguel de Tucumán, Vol. 6, p. 221–243.

Legarreta, L., and H. J. Villar, 2011, Geological and geochemical keys of the potential shale resources, Argentina basins: Search and Discovery Article 80196, accessed April 10, 2019, http://www.searchanddiscovery.com/pdfz/documents/2011/80196legarreta/ndx_legarreta.pdf.html

Lerche, I., and W. Narr, 1986, Estimating subsurface fracture density in core: Effects resulting from variable fracture spacing: SPE Formation Evaluation, v. 1, p. 249–258, SPE-13300-PA, DOI: 10.2118/13300-PA.

Llambías, E. J., and C. W. Rapela, 1989, Las volcanitas de Collipilli, Neuquén (378S) y su relación con otras unidades paleógenas de la cordillera: Revista de la Asociación Geológica Argentina, v. 44, p. 224–236.

Loucks, R. G., R. M. Reed, S. C. Ruppel, and D. M. Jarvie, 2009, Morphology, genesis, and distribution of nanometer-scale pores in siliceous mudstones of the Mississippian Barnett Shale: Journal of Sedimentary Research, v. 79, p. 848–861, DOI: 10.2110/jsr.2009.092.

Maerten, L., F. Maerten, F. Lejri, and P. Gillespie, 2016, Geomechanical paleostress inversion using fracture data: Journal of Structural Geology, v. 89, p. 197–213.

Maher, H. D. Jr., K. Ogata, and A. Braathen, 2016, Cone-in-cone and beef mineralization associated with the Triassic growth basin faulting and shallow shale diagenesis, Edgeøya, Svalbard: Geological Magazine, available on CJO2016, DOI: 10.1017/S0016756815000886.

Marchal, D., F. Sattler, and G. Köhler, 2016, Capítulo 14: Sierra Chata, *in* G. González, M. D. Vallejo, D. Kietzmann, D. Marchal, P. Desjardins, F. González Tomassini, L. Gómez Rivarola, and R. F. Domínguez, eds., Transecta

Regional de la Formación Vaca Muerta. Integración de sísmica, registros de pozos, coronas y afloramientos. Publicación especial del Instituto Argentino del Petróleo y del Gas (IAPG), Buenos Aires, p. 155–167.
Marchal, D., R. Manceda, R. F. Domínguez, and F. Sattler, 2020, Structural geology: Tectonic history, macrostructures, regional fault map, fault systems, second-order structures, and impact of the inheritance, *in* D. Minisini, M. Fantín, I. Lanusse Noguera, and H. A. Leanza, eds., Integrated geology of unconventionals: The case of the Vaca Muera play, Argentina: AAPG Memoir 121, p. XX–XX.
Marchese, H., 1971, Litoestratigrafía y variaciones faciales de las sedimentitas mesozoicas de la Cuenca Neuquina, Provincia del Neuquén, República Argentina: Revista Asociación Geológica Argentina, v. 26, no. 3, p. 343–410.
Marrett, R., O. J. Ortega, and C. M. Kelsey, 1999, Extent of power-law scaling for natural fractures in rock: Geology, v. 27, p. 799–802, DOI: 10.1130/0091-7613(1999)027<0799:EOPLSF>2.3.CO;2.
Marrett, R., J. F. W. Gale, L. Gomez, and S. E. Laubach, 2018, Correlation analysis of fracture arrangement in space: Journal of Structural Geology, v. 108, p. 16–33, DOI: 10.1016/j.jsg.2017.06.012.
Martinez, V., T. Musso, G. Pettinari, and A. Molina, 2017, Litofacies, mineralogía y caracterización de microfracturas naturales (venillas rellenas de calcita tipo beef) en el intervalo basal de la formación Vaca Muerta en el Bajo de Añelo, Cuenca Neuquina: 20° Congreso Geológico Argentino, San Miguel de Tucumán, Argentina, 7–11 August, Simposio Geología de la Formación Vaca Muerta, p. 85–90.
Maxwell, S. C., M. Mack, F. Zang, D. Chorney, S. D. Goodfellow, and M. Grob, 2015, Differentiating wet and dry microseismic events induced during hydraulic fracturing: Unconventional Resources Technology Conference, San Antonio, Texas, USA, 20–22 July, SPE-178585-MS, DOI: 10.2118/178585-MS.
Meissinger, V., and G. Lo Forte, 2014, El shale desde el punto de vista diagenético: el aporte volcánico en a la diagénesis temprana de la formación Vaca Muerta: 9° Congreso de Exploración y Desarrollo de Hidrocarburos, Simposio de Recursos No Convencionales, Mendoza, 3–7 November, p. 403–426.
Minisini, D., P. Desjardins, G. Otharán, M. Paz, D. Kietzmann, G. Eberli, C. Zavala, T. Simo, J. H. Macquaker and C. Heine, 2020, Sedimentology, depositional model, and implications for reservoir quality, *in* D. Minisini, M. Fantin, I. Lanusse Noguera, and H. A. Leanza, eds., Integrated geology of unconventionals: The case of the Vaca Muerta play, Argentina: AAPG Memoir 121, p. XX–XX.
Mitchum, R. M., and M. A. Uliana, 1985, Seismic stratigraphy of carbonate depositional sequences, Upper Jurassic–Lower Cretaceous, Neuquén Basin, Argentina, *in* O. R. Berg, and D. G. Woolverton, eds., Seismic stratigraphy II: An integrated approach to hydrocarbon exploration: AAPG Memoir 39, p. 255–274.
Monti, L. J., M. I. Suarez, A. R. Thompson, and L. Vega, 2013, Modeling vertical multifractured wells in Vaca Muerta shale oil play, Argentina, SPE Unconventionals Resources Conference, The Woodlands, Texas, USA, 10–12 April, DOI: 10.2118/164537-MS.
Mosquera, A., and V. A. Ramos, 2005, Intraplate deformation in the Neuquén embayment: 5° Congreso Argentino de Exploración y Desarrollo de Hidrocarburos, Actas 2, p. 193–202.
Narr, W., and J. Suppe, 1991, Joint spacing in sedimentary rocks: Journal of Structural Geology, v. 13, p. 1037–1048.
Olson, J. E., S. E. Laubach, and R. H. Lander, 2009, Natural fracture characterization in tight gas sandstones: Integrating mechanics and diagenesis: AAPG Bulletin, v. 93, p. 1535–1549.
Ortega, O. J., R. A. Marrett, and S. E. Laubach, 2006, A scale-independent approach to fracture intensity and average spacing measurement: AAPG Bulletin, v. 90, p. 193–208, DOI: 10.1306/08250505059.
Palacio, J. P., D. E. Hryb, and F. González Tomassini, 2018, Predicción de la distribución de beefs en la Formación Vaca Muerta: Un análisis integrado: 10° Congreso de Exploración y Desarrollo de Hidrocarburos, Mendoza, 5–9 November, Simposio de Recursos No Convencionales paper, accessed April 10, 2019, https://docplayer.es/120189913-Programa-actividades-tecnicas-sesiones-generales.html.
Pardo-Casas, F., and P. Molnar, 1987, Relative motion of the Nazca (Farallon) and South American plates since Late Cretaceous time: Tectonics, v. 6, no. 3, p. 233–248.
Passchier, C. W., and R. A. J. Trouw, 1996, Microtectonics: Berlin, Springer Verlag. 289 pp.
Patzek, T., F. Male, and M. Marder, 2014, A simple model of gas production from hydrofractured horizontal wells in shales: AAPG Bulletin, v. 98, no. 12, p. 2507–2529.
Pesicek, J. D., E. R. Engdahl, C. H. Thurber, H. R. DeShon, and D. Lange, 2012, Mantle subducting slab structure in the region of the 2010 M8.8 Maule earthquake (30–40°S), Chile: Geophysical Journal International, v. 191, p. 317–324.
Prokoph, A., G. A. Shields, and J. Veizer, 2008, Compilation and time-series analysis of a marine carbonate $\delta^{18}O$, $\delta^{13}C$, $^{87}Sr/^{86}Sr$ and $\delta^{34}S$ database through Earth history: Earth-Science Reviews, v. 8, no. 73, p. 113–133.
Ramos, V. A., M. Naipauer, H. A. Leanza, and M. E. Sigismondi, 2020, An exceptional tectonic setting along the Andean continental margin, *in* D. Minisini, M. Fantín, I. Lanusse Noguera, and H. A. Leanza, eds., Integrated geology of unconventionals: The case of the Vaca Muera play, Argentina: AAPG Memoir 121, p. XX–XX.
Rodrigues, N., P. R. Cobbold, H. Løseth, and G. Ruffet, 2009, Widespread bedding-parallel veins of fibrous calcite ('beef') in a mature source rock (Vaca Muerta Formation, Neuquén Basin, Argentina): Evidence for overpressure and horizontal compression: Journal of the Geological Society, v. 166, p. 695–709.
Rojas Vera, E. A., A. Folguera, G. Zamora Valcarce, G. Bottesi, and V. A. Ramos, 2014, Structure and development of the Andean system between 36° and 39°S: Journal of Geodynamics, v. 73, p. 34–52.

Rojas Vera, E. A., J. Mescua, A. Folguera, T. P. Becker, L. Sagripanti, L. Fennell, D. Orts, V. A. Ramos, 2015, Evolution of the Chos Malal and Agrio fold and thrust belts, Andes of Neuquén: Insights from structural analysis and apatite fission track dating: Journal of South American Earth Sciences, v. 64, p. 418–433.

Rutledge, J., X. Yu, S. Leaney, L. Bennett, and S. Maxwell, 2014, Microseismic shearing generated by fringe cracks and bedding-plane slip: SEG Annual Meeting, Society of Exploration Geophysicists, Denver, Colorado, USA, 26–31 October, SEG-2014-0896, accessed April 10, 2019, DOI: 10.1190/segam2014-0896.1.

Sagasti, G., A. Ortiz, D. Hryb, M. Foster, and V. Lazzari, 2014, Understanding geological heterogeneity to customize field development: An example from the Vaca Muerta unconventional play, Argentina: Unconventional Resources Technology Conference, Denver, Colorado, USA, 25–27 August, DOI: 10.15530/urtec-2014-1923357.

Santiago, M. F., R. S. Rauzi, G. A. Laffitte, and O. A. Alvarado, 2014, La Formación Vaca Muerta como objetivo exploratorio no convencional en la subcuenca de Picún Leufú, Neuquén, Argentina: 9° Congreso de Exploración y Desarrollo de Hidrocarburos, Simposio de Recursos No Convencionales, Mendoza, Argentina, 3–7 November, p. 275–314.

Scheuber, E., T. Bogdanic, A. Jensen, and K.-J. Reutter, 1994, Tectonic development of the North Chilean Andes in relation to plate convergence and magmatism since the Jurassic, *in* K.-J. Reutter, E. Scheuber, and P. Wigger, eds., Tectonics of the Southern Central Andes: Berlin, Springer, p. 121–139.

Shrivastava, K., and M. M. Sharma, 2018, Mechanisms for the formation of complex fracture networks in naturally fractured rocks: SPE Hydraulic Fracturing Technology Conference and Exhibition, The Woodlands, Texas, USA, 23–25 January, 13 p., DOI: 10.2118/189864-MS.

Sillitoe, R., 1977, Permo-Carboniferous, Upper Cretaceous, and Miocene porphyry copper-type mineralization in the Argentinian Andes: Economic Geology, v. 72, p. 99–103.

Somoza, R., 1998, Updated Nazca (Farallon)-South America relative motions during the last 40 my: Implications for mountain building in the central Andean region: Journal of South American Earth Sciences, v. 11, p. 211–215, DOI: 10.1016/S0895-9811(98)00012-1.

Spalletti, L. A., Z. Gasparini, G. Veiga, E. Schwarz, M. Fernandez, and S. Matheos, 1999, Facies anóxicas, procesos deposicionales y herpetofauna de la rampa marina titoniano-berriasiana en la Cuenca Neuquina (Yesera del Tromen), Neuquén, Argentina: Revista Geológica de Chile, v. 16, p. 109–123.

Spalletti, L. A., J. R. Franzese, S. D. Matheos, and E. Schwarz, 2000, Sequence stratigraphy of a tidally dominated carbonate–siliciclastic ramp: The Tithonian–Early Berriasian of the Southern Neuquén Basin, Argentina: Journal of the Geological Society, v. 157, no. 2, p. 433–446.

Stearns, D. W., 1968, Certain aspects of fracture in naturally deformed rocks: National Science Foundation Advanced Science Seminar in Rock Mechanics, p. 97–118.

Swart, P. K., 2000, The oxygen isotopic composition of interstitial waters: Evidence for fluid flow and recrystallization in the margin of the Great Bahama Bank, *in* P. K. Swart, G. P. Eberli, J. F. Malone, and J. F. Sarg, eds., Proceedings of the Ocean Drilling Program: Scientific Results, v. 166, College Station, Texas, 7 Ocean Drilling Program 2000, p. 91–98.

Swart, P. K., 2015, The geochemistry of carbonate diagenesis: The past, present and future: Sedimentology, v. 62, p. 1233–1304.

Tan, Y., and T. Engelder, 2016, Further testing of the bedding-plane-slip model for hydraulic-fracture opening using moment-tensor inversions: Geophysics, v. 81, no. 5, p. KS159–KS168, DOI: 10.1190/geo2015-0370.1.

Tenaglia, M., R. Weger, G. Eberli, L. E. Rueda Sánchez, L. Rodriguez Blanco, and P. Swart, 2017, TOC distribution and prediction in the Vaca Muerta Formation, Neuquén Basin, Argentina: AAPG Annual Convention and Exhibition, Houston, Texas, USA, 2–5 April, AAPG Datapages/Search and Discovery Article 90291, accessed April 10, 2019, http://www.searchanddiscovery.com/abstracts/html/2017/90291ace/abstracts/2611932.html.

Tobin, K. J., K. R. Walker, D. M. Steinhauff, and C. I. Mora, 1996, Fibrous calcite from the Ordovician of Tennessee: Preservation of marine oxygen isotopic composition and its implications: Sedimentology, v. 43, p. 235–251.

Ukar, E., R. G. Lopez, A. Fall, R. Manceda, J. F. W. Gale, and S. E. Laubach, 2017a, Vertical fractures and a new type of kinematic indicator in bed-parallel veins (beef) in the Vaca Muerta Formation at Arroyo Mulichinco, Neuquén Basin: 20° Congreso Geológico Argentino, Simposio Geología de la Formación Vaca Muerta, San Miguel de Tucumán, 7–11 August, p. 163–165.

Ukar, E., R. G. Lopez, J. F. W. Gale, S. E. Laubach, and R. Manceda, 2017b, New type of kinematic indicator in bed-parallel veins, Late Jurassic–Early Cretaceous Vaca Muerta Formation, Argentina: E-W shortening during Late Cretaceous vein opening: Journal of Structural Geology, v. 104, p. 31–47.

Ukar, E., R. G. Lopez, S. E. Laubach, J. F. W. Gale, R. Manceda, and R. Marrett, 2017c, Microfractures in bed-parallel veins (beef) as predictors of vertical macrofractures in shale: Vaca Muerta Formation, Agrio Fold-and-Thrust Belt, Argentina: Journal of South American Earth Sciences, v. 79, p. 152–169, DOI: 10.1016/j.jsames.2017.07.015.

Ukar, E., S. E. Laubach, and J. N. Hooker, 2019, Outcrops as guides to subsurface natural fractures: Example from the Nikanassin Formation tight-gas sandstone, Grande Cache, Alberta foothills: Marine and Petroleum Geology, v. 103, p. 255–275, DOI: 10.1016/j.marpetgeo.2019.01.039.

Urien, C. M., and J. J. Zambrano, 1994, Petroleum systems in the Neuquén Basin, Argentina, *in* L. B. Magoon, and W. G. Dow, eds., The petroleum system—From source to trap: AAPG Memoirs 60, p. 513–534.

Varela, R. A., D. Marchal, S. Cuervo, E. F. Lombardo, Y. S. Perl, D. E. Hryb, P. Pateti, and O. Nielsen, 2020, Geomechanics: Pressure, stress-field, and hydraulic fractures, *in* D. Minisini, M. Fantín, I. Lanusse Noguera, and H. A. Leanza, eds., Integrated geology of unconventionals: The case of the Vaca Muera play, Argentina: AAPG Memoir ###, p. XX–XX.

Vergani, G. D., A. J. Tankard, H. J. Belotti, and H. J. Welsink, 1995, Tectonic evolution and paleogeography of the Neuquén basin, Argentina, *in* A. J. Tankard, R. Suarez, and H. J. Welsink, eds., Petroleum basins of South America: AAPG Memoir 62, p. 383–402.

Wang, Q., 2016, Characterization of bedding-parallel fractures in shale: Morphology, size distribution and spatial organization, Master's thesis, The University of Texas at Austin, 282 p.

Warpinski, N. R., R. C. Kramm, J. R. Heinze, and C. K. Waltman, 2005, Comparison of single- and dual-array microseismic mapping techniques in the Barnett shale: SPE Annual Technical Conference and Exhibition, Dallas, Texas, USA, 9–12 October, SPE-95568-MS, p. 1–10, DOI: 10.2118/95568-MS.

Weger, R. J., S. T. Murray, and D. F. McNeil, 2017, Clumped isotope paleothermometry of calcite beef in the Vaca Muerta Formation, Neuquén Basin: 20° Congreso Geológico Argentino, San Miguel de Tucumán, Argentina, 7–11 August, Simposio Geología de la Formación Vaca Muerta, p. 185–190.

Weger, R. J., S. T. Murray, D. F. McNeil, P. K. Swart, G. P. Eberli, L. Rodriguez Blanco, M. Tenaglia, and L. Rueda, 2019, Paleo thermometry and distribution of calcite beef in the Vaca Muerta Formation, Neuquén Basin, Argentina: AAPG Bulletin, v. 103, no. 4, p. 931–950. DOI: 10.1306/10021817384.

Wilkins, S., V. Mount, K. Mahon, A. Perry, and J. Koenig, 2014, Characterization and development of subsurface fractures in the Marcellus Formation, Appalachian Plateau, north-central Pennsylvania: AAPG Bulletin, v. 98, no. 11, p. 2301–2345.

Wu, H., and D. Pollard, 1995, An experimental study of the relationship between joint spacing and layer thickness: Journal of Structural Geology, v. 17, p. 887–905.

Wu, K., and J. E. Olson, 2016, Numerical investigation of complex hydraulic-fracture development in naturally fractured reservoirs: SPE Production and Operation, v. 31, p. 300–309.

Zamora Valcarce, G., T. Zapata, D. del Pino, and A. Ansa, 2006, Structural evolution and magmatic characteristics of the Agrio fold-and-thrust belt, *in* S. M. Kay, and V. A. Ramos, eds., Evolution of an Andean margin: A tectonic and magmatic view from the Andes to the Neuquén Basin (358–398S lat.): Geological Society of America Special Papers 407, p. 125–145.

Zamora Valcarce, G., T. Zapata, V. A. Ramos, F. Rodríguez, and L. M. Bernardo, 2009, Evolución tectónica del frente andino en Neuquén: Revista de la Asociación Geológica Argentina, v. 65, no. 1, p. 192–203.

Zanella, A., P. R. Cobbold, G., Ruffet, and H. A. Leanza, 2015, Geological evidence for fluid overpressure, hydraulic fracturing and strong heating during maturation and migration of hydrocarbons in Mesozoic rocks of the northern Neuquén Basin, Mendoza Province, Argentina: Journal of South American Earth Sciences, v. 62, p. 229–242.

Zanella, A., P. R. Cobbold, N. Rodrigues, H. Loseth, M. Jolivet, F. Gouttefangeas, and D. Chew, 2020, Source rocks in foreland basins: A preferential context for the development of natural hydraulic fractures: AAPG Bulletin, in press.

Zapata, T., I. Brissón, and F. Dzelalija, 1999, La estructura de la faja plegada y corrida andina en relación con el control del basamento de la Cuenca Neuquina: Buenos Aires, Boletín de Informaciones Petroleras, v. 60, p. 113–121.

Zeller, M., S. B. Reid, G. P. Eberli, R. J. Weger, and J. L. Massaferro, 2015, Sequence architecture and heterogeneities of a field—Scale Vaca Muerta analog (Neuquen Basin, Argentina)—From outcrop to synthetic seismic: Marine and Petroleum Geology, v. 66, p. 829–847, DOI: 10.1016/j.marpetgeo.2015.07.021.

Zhang, F., E. Dontsov, and M. Mack, 2017, Fully coupled simulation of a hydraulic fracture interacting with natural fractures with a hybrid discrete-continuum method: International Journal for Numerical and Analytical Methods in Geomechanics, DOI: 10.1002/nag.2682.

Zhang, X., R. G. Jeffrey, and M. Thiercelin, 2009, Mechanics of fluid-driven fracture growth in naturally fractured reservoirs with simple network geometries: Journal of Geophysical Research, v. 114, B12406, DOI: 10.1029/2009JB006548.

Zonenshayn, L. P., L. A. Savostin, and A. P. Sedov, 1984, Global paleogeodynamic reconstructions for the last 160 million years: Geotectonics, v. 18, p. 181–195.